Vilnius University
Physics Faculty
Laser Research Center

Diana Gonzalez-Hernandez

MEASUREMENTS OF EFFECTIVE OPTICAL REFRACTIVE INDEX FOR 3D MICROELEMENTS

Master thesis

Laser Technologies
study program

Student	Diana Gonzalez-Hernandez
Supervisor	Prof. Mangirdas Malinauskas
Consultant	Dr. Darius Gailevičius
Reviewer	Dr. Andrejus Michailovas
Director	Prof. Aidas Matijošius

Vilnius 2021

Content

Introduction

The two-photon lithography (TPL) technique has shown versatility for the fabrication of true three-dimensional (3D) micro structures in the last two decades [1]. This technology has emerged taking the advantage of two-photon absorption (TPA) by a photoresin material and by point-by-point fabrication process. By using TPL technique we are able to create true 3D novel structures with resolution in the micro range. The photopolymerization technique owns a wide potential in the fabrication of 3D functional micro structures for different applications [2].

Novel microstructures for optical applications are being designed and fabricated by using TPL. The freedom in fabrication that this technique provides allows applications such as high numerical aperture array of micro lenses [3], reversible birefringence micro structures [4], [5], gradient index (GRIN) micro optic structures [6], photonic crystal beam splitter [7], meta lens for optical trapping [8], as well as apochromat elements [9] and many others.

Notwithstanding the demonstration of plenty optical microelements fabricated by TPL, there is still a need of wider understanding of optical properties, as it is the refractive index (RI) of photopolymer materials after the polymerization process. This lack of knowledge limits further advances in designing and optimization of novel optical microelements. Although recent studies of optical properties from ultraviolet (UV) and near infrared (NIR) range have been performed for common materials processed by TPL, these were limited to the study of two-dimensional (2D) microstructures [10]. Such studies provide information of the intrinsic RI of the material but it could differ from the effective RI.

The effective RI of the structure became an interesting parameter because the optical structures can manipulate the light flow passing through them. This parameter represents the effective property of the optical element which delays the light and affects its behaviour due to its geometry, surface homogeneity and shape.

To optimize the imagining performance of optical microelements detailed knowledge of the effective RI of the material of elements fabricated by TPL is fundamental. Different methods for RI characterization have been used, such as interferometry [6], ellipsometry [10], coupler prism m-lines [11], and critical angle by total internal reflection [12]. The differences of these methods are explained in the following work. However, these techniques can be applied only with 2D specimens limiting their application for different structures. For a 3D complex micro structure a different approach to retrieve the RI is required. This works presents a RI measurement technique based on the index-matching (IM) oils method [13]. The versatility of the proposed method could lead to accurate measurements of RI of complex 3D structures and not

only 2D flat structures. On the other hand, by exploiting the optical behaviour of microlenses, the effective RI can be retrieved from the dimensions and focal length of the element.

The aim of this project is to retrieve the RI of microelements, under 100 μm, out of hybrid organic-inorganic prepolymer (SZ2080™) fabricated by TPL using two different approaches: index-matching oils method and focal length measurements. To achieve this goal design of elements and the writing method is required. We predict the dependence of the RI on fabrication parameters by index-matching method for the microcuboids and focal length (f) measurement of spherical microlenses.

To achieve this goal the following tasks have been set:

1. To fabricate micro cuboids by Layer-by-Layer writing method by TPL.
2. To fabricate spherical micro lenses of same geometrical dimensions varying the exposure dose used by TPL.
3. To retrieve the RI of the micro prisms by the proposed index-matching oil method in collaboration with Prof. Brasselet's group in Laboratoire Ondes et Matière d'Aquitaine, CNRS, Bordeaux.
4. To retrieve the RI of the spherical lenses from experimental values of focal length measurements.
5. To evaluate the dose dependence behaviour of the RI of fabricated micro structures by TPL.

1 Literature Review

1.1 Laser Direct Writing Technique

The laser direct writing (LDW) is a technique highly studied and used during the last 20 years due to its versatility of custom-shaped 3D microstructure with lateral and axial resolution beyond the diffraction limit of optical wavelengths. The LDW technique in the form of the multiphoton polymerization is based on the simultaneous absorption of two or more photons of the same frequency in photosensitive molecules that subsequently undergo a radicalization process. The photogenerated radicals induce a cross-linking of polymeric materials. Because of the nonlinear interaction between the light and the photoresin, the photochemical reaction is highly confined inside the volume of the tightly focused laser beam. This allows the fabrication of 3D microstructures by point-to point photostructuring of the prepolymer. The smaller fabricated element is called voxel, volumentric pixel, formed in the area of the focused beam and following the programed path of the beam leads to the creation of complex micro structures. The photopolymerized areas of the material becomes insoluble in organic solvents while the unexposed prepolymer is disolved and washed out.

The process can be divided in four main stages and it is shown in Fig. 1: (1) sample preparation, (2) fabrication process, (3) development stage and (4) characterization of the fabricated microstructure.

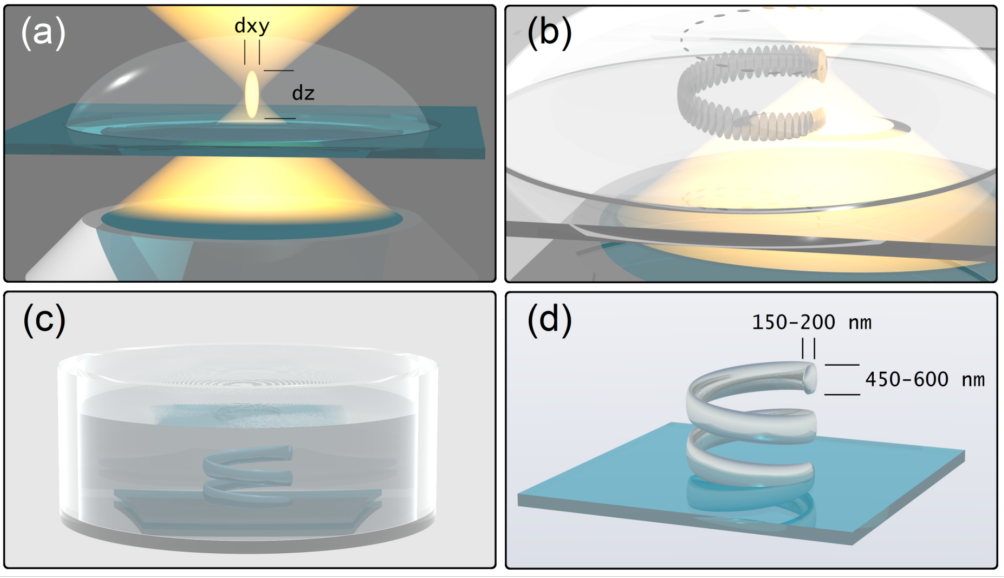

Fig. 1 Principles of LDW. a) TPP in the focus region of a tightly focused fs pulsed beam. b) Point-by-point fabrication by path beam followed in the photoresist material. c) Chemical development process washes out the non-pholymerized material. d) Self-standing microstructure attached to glass substrate [2].

1.2 Photopolymerization Mechanism

In the TPL process, a polymer structure is formed by nonlinear absorption of two-photons in a prepolymer material. Ultrashort pulses are tightly focused in a photopolymer though a high numerical aperture (NA) objective (1.25-1.4). Since the photopolymer is transparent in the VIS-NIR spectral range, the photopolymerization process occurs within the vicinity of the focused beam inside the material [2].

When a high quality factor beam ($M^2 \approx 1$) is focused within a material, the multi photon absorption process takes place if the photon density within the focal volume exceeds a certain threshold value. The electron transition is induced by N photons with $1/N$ of the energy required by the gap between the two energy levels. In order to obtain a photopolymerization voxel smaller than the one predicted by the optical diffraction limit defined by the wavelength and the NA of the beam, only the central part of the Gaussian beam should be set above the intensity threshold. In this way, the multiphoton absorption will take place within the voxel because of the nonlinear dependence on I^N, quadratic in the case of TPA. The simultaneous absorption of two-photons involves a virtual state which is created by the first photon and the second photon is absorbed if it arrives within the virtual state. This condition is fulfilled when ultra short femtosecond pulses are used [14].

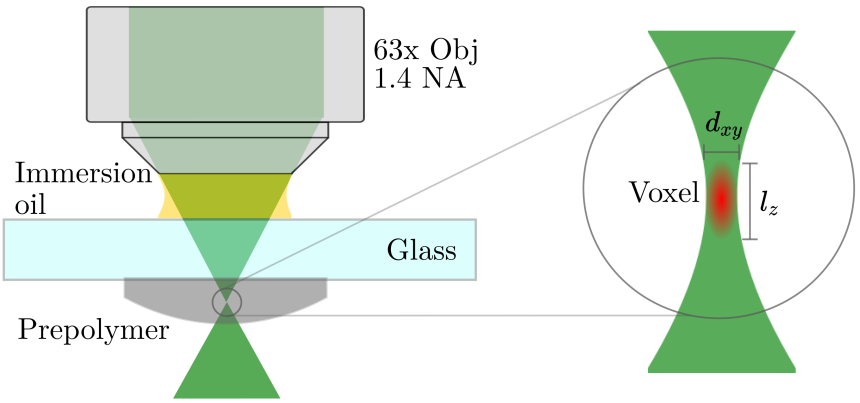

Fig. 2 Laser direct writing by TPL schematic by VIS radiation. The VIS beam is focused by a high NA objective (oil immersed) within the prepolymer. The intensity at the focus overpass the intensity threshold and polymerize the material.

The intensity distribution plays a key role in the spatial confinement of TPA [1]. Varying the light intensity distribution allows fine tuning of the voxel dimensions. The fabrication window is defined as the ratio of the intensity of the material optical damage and the threshold intensity required for polymerization. Fig. 3 shows a relation between input intensity and voxel dimensions over an intensity threshold required for starting the polymerization process [14].

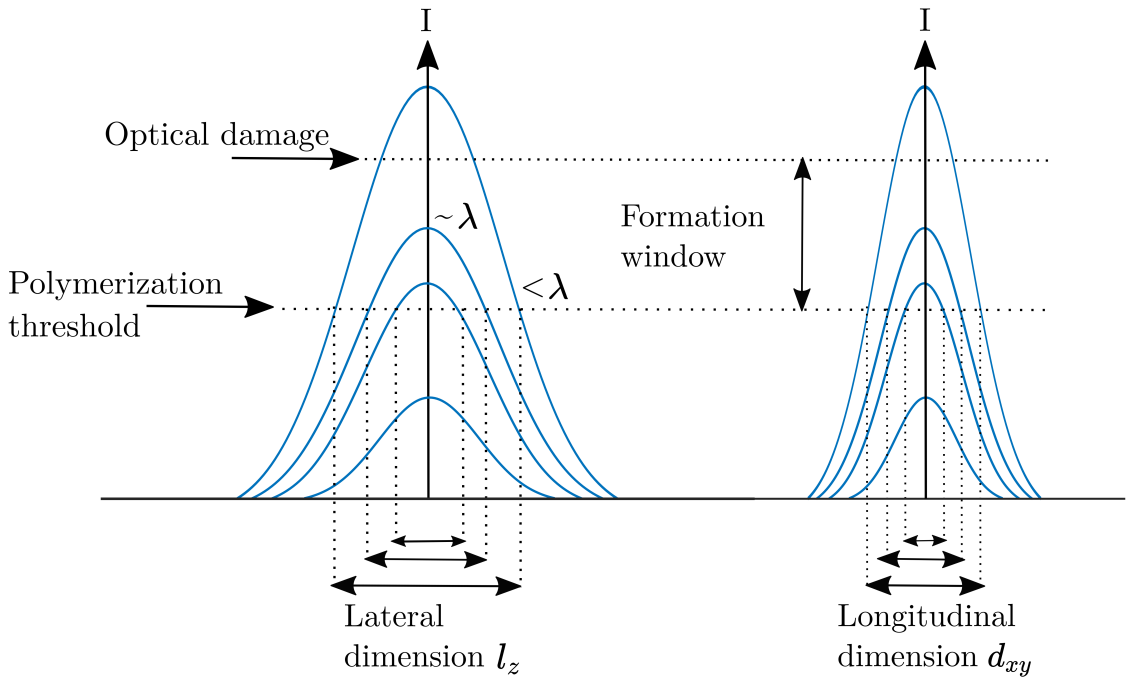

Fig. 3 Intensity distribution at the focal spot of the light beam. The polymerization occurs only for intensities over the threshold value. If the intensity is too high (above 10 $\mathbf{TW/cm^2}$)would lead to optical damage of the material. The dimensions of the voxel can be approximated as the size of the focal spot of the beam. [14].

In order to enhance the photopolymerization reaction, photo initiators (PI) are mixed in the photoresin up to few weight percent (wt%). These are UV or VIS radiation sensitive molecules which absorption of light form reactive components capable of starting the polymerization process, which occurs via opening of chemical bonds (formation of radicals) and subsequent crosslinking [15]. These PIs have a lower dissociation energy, around 3 eV, than monomers which is around 4 eV for UV/VIS light [1].

The photopolymerization process is defined by three main steps: initiation, chain propagation and termination. The first step is the absorption of high intensity radiation and generation of free radicals, which interact with the monomers, by the PIs. This process occurs because the photoinitiator is excited from its electronic singlet ground state, S_0 to the excited singlet manifold S_1; it then relaxes by intersystem crossing ISC to the triplet state T_1 and forms the free radicals as show in Fig. 4. The chain-propagation is the expansion of the monomer-radicals reaction. Finally, the termination is when two radicals meet and stops the process [14]. The photopolymerization will follow the path of the beam within the photoresin, allowing the creation of 3D free-form micro structures with a resolution given by the voxel dimensions. We can approximate the voxel dimensions, d_{xy} and l_{z} as axial and longitudinal, with the spot size

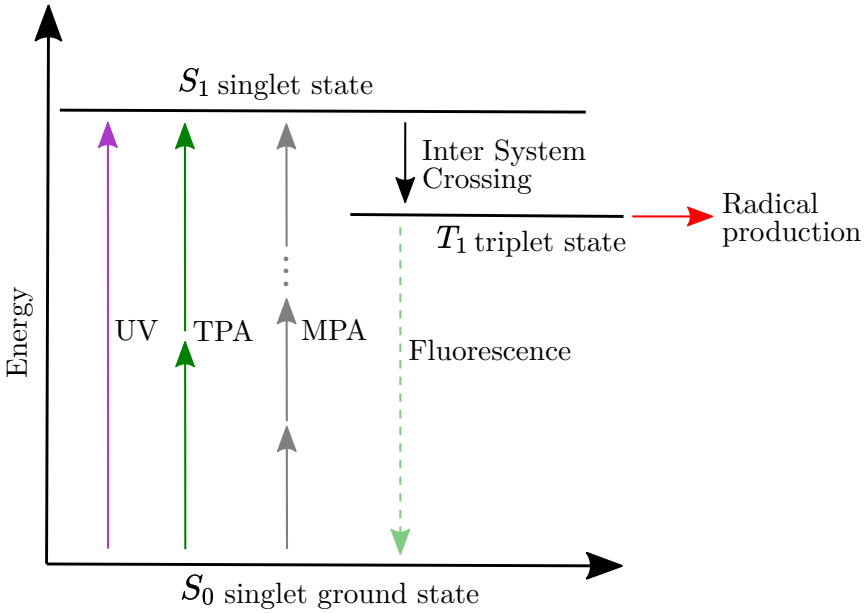

Fig. 4 Energy diagram for photopolymerization process. For a single photon a polymerization occurs at the UV wavelength range. Multiphoton poymerization occurs by the simultaneous absorption of multiple photons of lower energy that together excites the electron to a higher energy state.

of the beam that can be calculated from Eq. 1 and Eq. 2, which depend on the wavelength of the beam λ, and the NA of the microscope objective lens used to focus the beam within a prepolymer of RI n_p.

$$d_{\mathrm{xy}} = \frac{1.22\lambda}{NA}, \tag{1}$$

$$l_{\mathrm{z}} = \frac{1.22 n_p \lambda}{NA^2}. \tag{2}$$

The multiphoton absorption rate is proportional to the irreversible polymerization reaction above the intensity threshold value required I_{th}. Since the voxel takes the shape of the intensity distribution of the focused laser beam on the focal spot, we can approximate its dimensions considering the order of absorption nonlinearity, $N = 2$ in case of two-photon polymerization (TPP) as shown in Eq. 4 and Eq. 5, where $w_0 = (0.61M^2\lambda)/NA$ is the waist of the Gaussian beam and $z_R = \pi w_0^2/\lambda$ means the Rayleigh distance [14]. The intensity of the beam I is related to the fabrication optical laser power P as in the following way:

$$I = \frac{2PT}{f w_0^2 \pi \tau}, \tag{3}$$

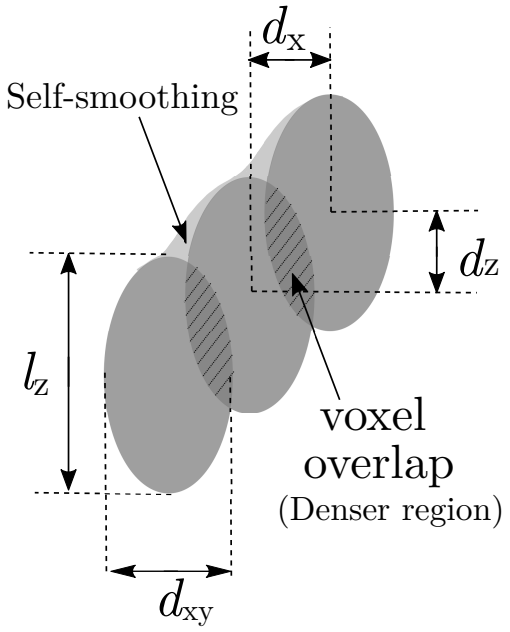

Fig. 5 Voxel overlap diagram of a voxel of axial and longitudinal dimensions l_z and d_{xy} and beam displacement d_x and d_z.

where T is the transmittance of the objective, f the repetition rate and τ the pulse duration of the laser.

$$d_{xy} = w_0 \sqrt{2 \frac{1}{N} \ln\left(\frac{I}{I_{th}}\right)}, \quad (4)$$

$$l_z = 2 z_R \sqrt{\left(\frac{I}{I_{th}}\right)^{\frac{1}{N}} - 1}. \quad (5)$$

The surface roughness depends on the voxel overlap δ which will smoothing the .

When the axial and lateral scanning steps become smaller, the overlaping increases for same voxel dimensions. For the fabrication of different structures, lines formed out of individual voxels are usually used. We can calculate the line volume considering the dimensions d_{xy} and l_z, of individual voxel approximated to an ellipsoid and the scanning velocity. The Eq.6 considers the area of the voxel cross-section and the translation velocity v_t [16].

$$V_l = \frac{\pi}{4} d_{xy} l_z v_t. \quad (6)$$

The degree of voxel overlap can be expressed as the product of voxel displacement in axial and lateral directions [17]. Considering volumetric lines, it is possible to calculate the volumetric overlapping in the fabricated structure.

1.3 RI Measurement Methods

Several strategies have been implemented to obtain the RI of materials treated by TPP. Advantages and disadvantages of different methods are presented below, as well as the main limitations of these methods for the measurement of the RI of complex 3D microstructures fabricated by TPL. A proposed method is presented at the end of the chapter that pretends to overcome the limitations in size and complexity of the micro structure.

1.3.1 Coupler Prism m-lines

Totally reflecting prism coupler (TRPC) also called m-line technique has been used for the determination of the RI of thin layers of photo sensitive materials used for TPP in the shape of homogeneous isotropic single-layer optical waveguides. This method is used to determinate optical properties of ultra low shrinkage hybrid material SZ2080™ [18] and the losses in multilayer coatings [19] .

The m-lines appears for the different incident directions corresponding to the coupling of light in the waveguide. Increasing the coupling between the prism and the waveguide the m-lines get broader and shift. Fig. 6 shows a schematic of the device using a isosceles prism [11]. The coupling of an incident laser beam by a prism into the planar waveguide is controlled by the incident angle θ_p of the beam on the prism base.

Under total internal reflection conditions, strong coupling can occur via resonant frustrated total reflection which is via the evanescent waves in the air layer. This coupling occurs when resonant conditions inside the waveguide are met and leads to a finite number of discrete incidences of the laser beam called synchronism angles θ_{sync}. The coupling is observed experimentally through the appearance of a dark line in the reflected beam, associated to a bright line next to it. The method measure synchronism angles of such m-lines and leads to the calculation of the RI and thickness of the waveguide and fitting them in the dispersion equation of the planar dielectric guide [20].

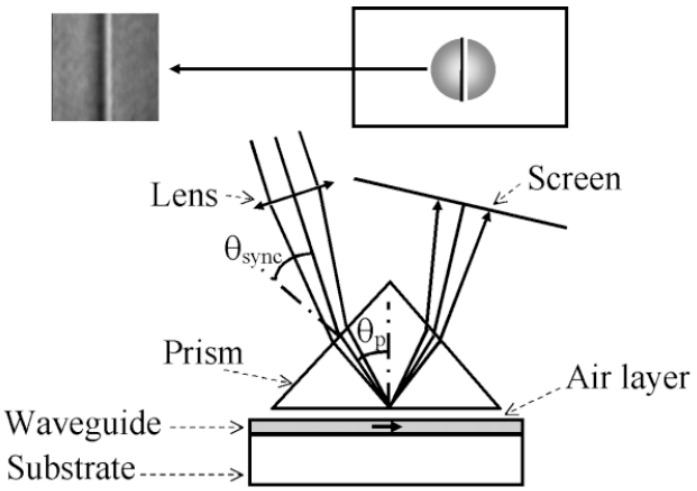

Fig. 6 Schematic representation of the TRPC and CCD camera for m-lines [11].

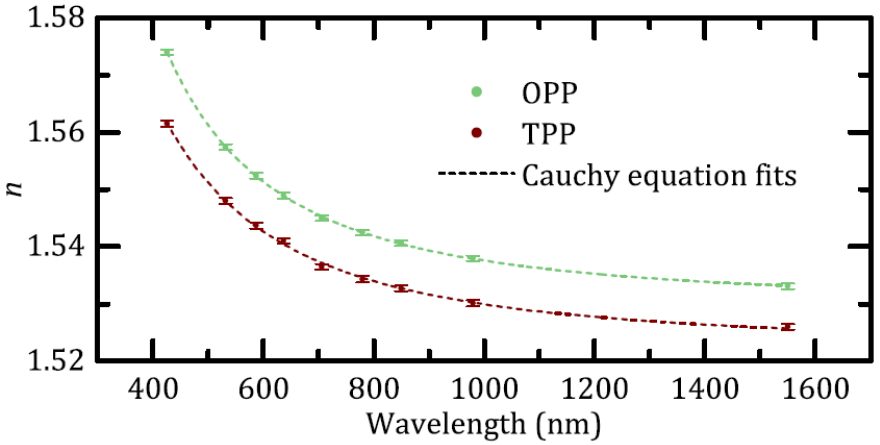

Fig. 7 Measured dispersive RI of IP/Dip layers for OPP and TPP. The results obtained match as the ones presented in Ref. [21].

The guided waves technique can be applied to the characterization of complex guiding structures such as an inhomogeneous layer with a particular index profile or even a multilayer system or to study the anisotropies of index of the layers. When the temperature changes, the different guided modes propagation constants are modified and the corresponding m-lines shifted and knowing the temperature allows the calculation of the RI and the thickness of the isotropic layer [22].

Commercial devices have reached an accuracy around ± 0.0005 for the RI value. The sample require a minimum thickness to support modes and a reference material with known RI. A Cauchy model can be used for the dispersion curve as shown in Fig. 7 and the air layer thickness between the reference material and the sample has to be taking into account for accurate results [21].

1.3.2 Ellipsometry

Ellipsometry is a technique commonly used to measure the thickness and RI or homogeneous and isotropic thin filmd, single or multilayer, from few Å to several micrometers. The measurements are done by sending a polarized light beam on a sample and measuring the intensity of the reflected light at large angles of incidence after using a second polarizator as analyzer. The linearly polarized light usually change to an elliptical polarized light after the sample, from this the origin of the name.

The measured signal is the change in polarization as the incident radiation interacts with the material sample. The polarization changes are quantifies by the amplitude ratio Ψ and the phase difference Δ. The basic setup for an ellipsometer consists in light source, polarization state generator, a sample, polarizator state detector and a light detector as shown in Fig. 8. The ellipsometer measures the complex reflectance ratio ρ of a system parameterized by Ψ and Δ and linked to the normalized reflection amplitudes [23] of s and p-polarization incident light as in Eq. (7).

$$\rho = \frac{r_{\mathrm{p}}}{r_{\mathrm{s}}} = \tan(\Psi) \cdot e^{i\Delta} = \rho_{\mathrm{r}} + i\rho_{\mathrm{i}} \tag{7}$$

Ellipsometry results are model dependent and accurate models can be made using classical electromagnetic theory based on Maxwell's equations [24]. These models can be used to obtain the RI and thickness of the materials and some examples are the Cauchy model [25] and parametrized dielectric function model using Gaussian, Lorentz and Tauc-Lorentz broadening [10] to describe the optical responses of the sample by single-photon polymerization (SPP).

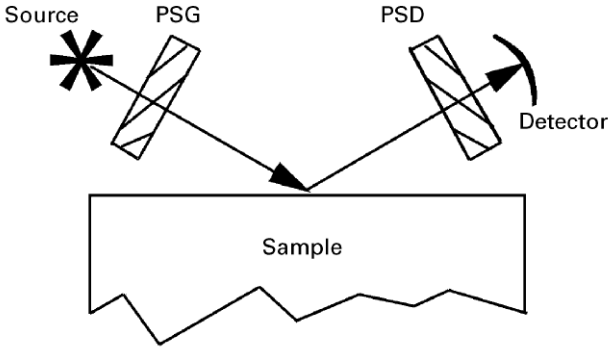

Fig. 8 Simple schematic of ellipsometry setup including a polarization state generator (PSG) and polarization state detector (PSD) [24].

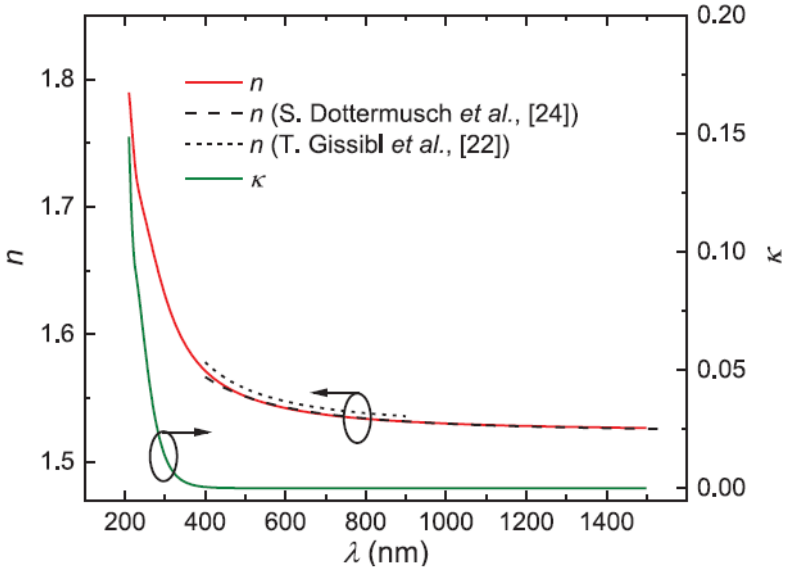

Fig. 9 Best-fit model RI n (red solid line) and extinction coefficient k (green line). TPP (dashed lines) and SPP (dotted lines) [10].

Some advantages are that 16 parameters can be measured for each wavelength. The measure of the ratio of intensity which decrease the impact of intensities instabilities by the light source or atmospheric absorption. The principal attraction is that complex RI can be measured using this technique which makes it superior to reflectivity measurements while studying anisotropic materials. Accurate results were obtained in comparison with previous values with different techniques but for an spectral range from 210 nm to 1500 nm with a fixed angle of incidence of 65° are shown in Fig. 9. A Cauchy model is used for fitting, requires prior information of RI and thickness and films must have good surface quality to avoid scattering [10].

1.3.3 Reflectrometry

Another method to retrieve the RI of a thin film is by the critical angle of total internal reflection α and it has been measured by using a modified Pulfrich refractometer [12]. The setup shown in Fig. 10 consist in a linearly polarized light of a laser diode directed through an astronomical telescope onto the base of the highly refractive N-SF11 prism. The reference material is N-BK7 plate which is optical bonded by pressure and the prism is coated with an approximately 2 mm layer of photo resist next to it. The angle of incidence is controlled onto the base of the prism by a mirror in a rotation mount and can be found using trigonometric functions in Snell's law, Eq. (8). The astronomical telescope has f_1 and f_2 and ensures nearly no walk on the back of the prism. The reflection intensity is collected by a photo diode guided with a second astronomical telescope [26].

$$\theta(\alpha) = 60^\circ + \arcsin\left[\frac{n_1}{n_2}\sin\left(\arctan\left(\frac{f_1}{f_2}\tan(2\alpha)\right)\right)\right] \approx 60^\circ + \frac{n_1}{n_2}\frac{f_1}{f_2}2\alpha. \tag{8}$$

To calculate the critical angle we have to obtain the point of the critical angle of the prism/photo resist interface and as well as the prism/BK7 glass plate for calibration. The critical angle is given by Eq. (9) where n_1 is the RI of the photo resist and n_2 of the prism. The total reflection condition is $n_1 > n_2$ and for angles larger than θ_c the light is completely internally reflected.

$$\theta_c = \arcsin\left(\frac{n_2}{n_1}\right). \tag{9}$$

$$R_s = \left| \frac{n_1 \cos\theta_1 - \sqrt{n_2^2 - n_1^2 \sin^2\theta_1}}{n_1 \cos\theta_1 + \sqrt{n_2^2 - n_1^2 \sin^2\theta_1}} \right|^2 \tag{10}$$

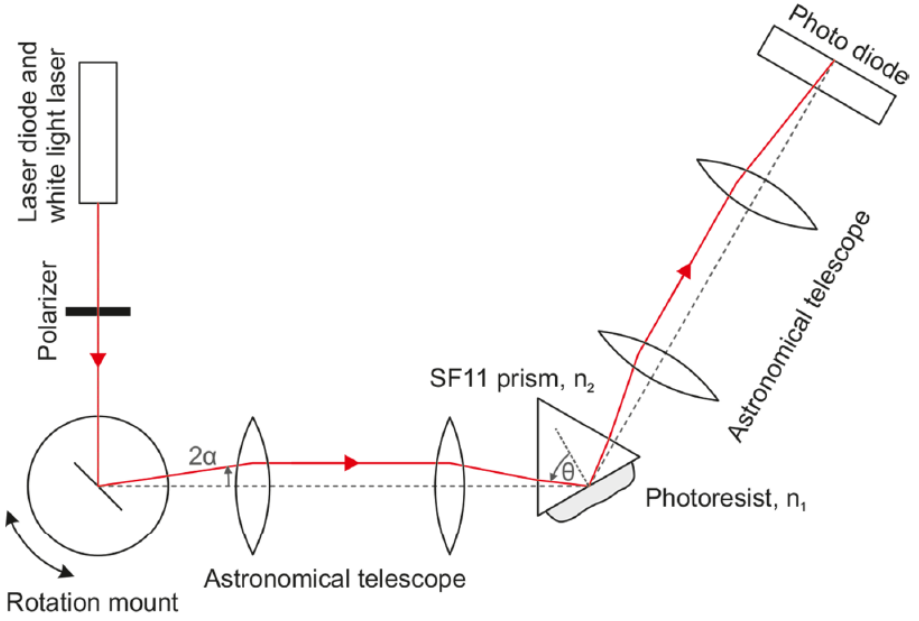

Fig. 10 Modified Pulfrich refractometer setup [26].

The critical angle is determinate from the angular reflection curves for an specific photo resist as shown in Fig. 11. This method can reach an accuracy of 5×10^{-4} for the RI measurement [12]. This method is limited by the dimension of the sample since it is only suitable for 2D structures.

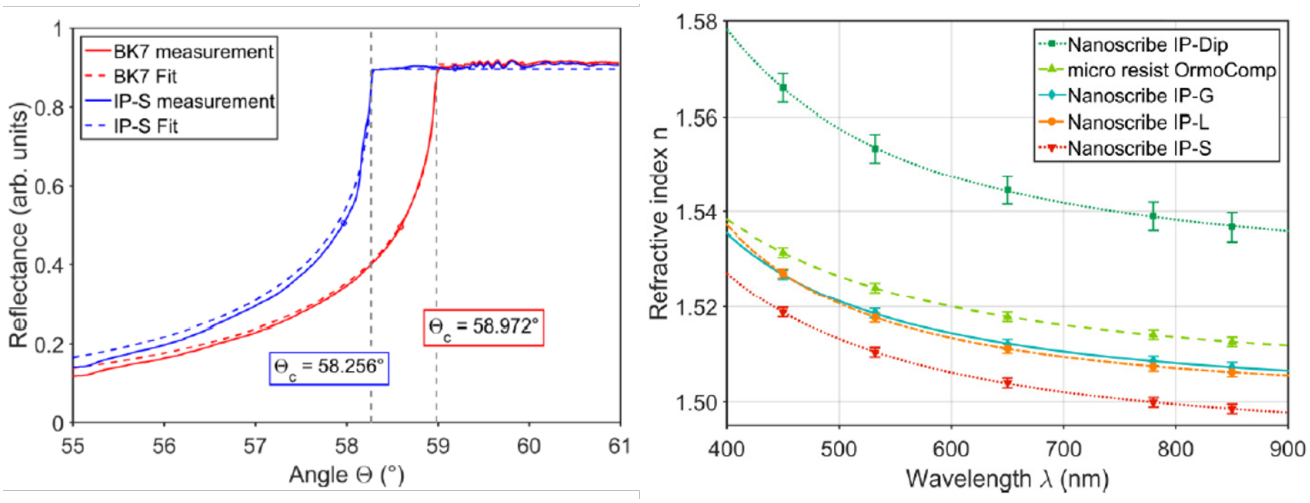

Fig. 11 Measurements of the critical angle of the total internal reflection of s-polarized light for OrmoComp resin and BK7 glass at wavelength of 850 nm [12].

1.3.4 Interferometry

Interferometric techniques can measure small changes in RI of a material. An interferometer splits the light into two beams using a beamsplitter, delays them by unequal distances and recombine them to detect the intensity of the superposition of these beams. This intensity is sensitive to the phase ϕ that depends on the differences traveled by the waves. A Michaelson interferometer is used to measure the changes in a trapezoidal prism fabricated by TPL as shown in Fig. 12. The intensity of the superposed beam is collected as an interference pattern from the beam propagating through the microstructure by adjusting one of the mirrors, with straight equally spaced lines near the beam axis. The relation within the intensity and its phase gives the change in RI in respect to the reference, evaluated with the Eq. (11). In order to obtain the distance between interference fringes d, the intensity is measured in the same line as shown in Fig. 12 c), fit with a sine function and calculate the distance between peak maxima [6].

$$\Delta n = \frac{\phi \lambda}{2\pi h}. \tag{11}$$

The condition $w_0 \gg b$ ensures the plane wave interaction, where w_0 is the beam size and b is the longest side of the prism. The phase can be calculated by $\phi = \Delta d/d$ where d is the period of the interference fringes and h represents the height of the prism. The results showed changes in the SZ2080™ polymer up to $1.16 \pm 0.12 \times 10^{-2}$ with sensitivity of around 0.0010 for a gradient index structure [6].

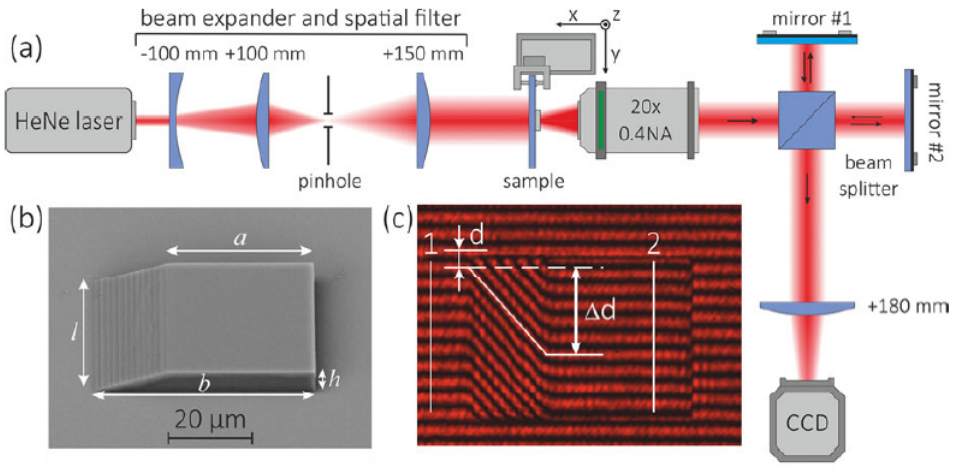

Fig. 12 a) Experimental Michaelson interferometer setup. b) SEM image of trapezoidal prism at 45° view. c) Interference pattern between the laser beam through the structure and the reference (air) [6].

Such methodology shows an accurate technique to calculate the RI of microstructures fabricated by TPL but it is limited a 2.5D simple structures which is not suitable for optical microelements.

1.3.5 Index-Matching Oils

A different approach is proposed, IM oil materials can be used for the investigation of complex geometry with unknown RI. This oil immersion technique is also used in light microscopy to increase the resolution and the NA of the objective lens as well as in fluid dynamics to minimise reflection, refraction, and diffraction than occurs in system with many interfaces and give access to previously inaccessible regions for optical measurements [13].

This method consist in immersing a specimen in a liquid with known RI. When the RI of the liquid matches the one of the specimen, it becomes transparent to light. Several IM oils should be used to compare the RI of the specimen. In order to optimize this process, an interpolation of the maximum transmission can be applied to a solid immersed in liquids with different RI. Previous work has used this method to find the RI of poly(vinylidene fluoride) (PVDF) films presenting a reproducibility of ± 0.003 and accuracy better than 0.01. The accuracy of the method highly depends on the immersion liquid range. A way to reduce the number of oil liquids used and increasing the accuracy of the method is by a mathematical fit of the transmission spectral curve. Performing transmission measurements by a UV/VIS spectrometer, it is possible to retrieve the values of the RI of the specimen of interest. In the Eq. (12) is expressed that the match between both RI is done when the transmission $\boldsymbol{T}$ is maximum. The transmission for light incident perpendicular to the sample surface is related

to the RI of the sample n_s and the immersion oils as surrounding medium n_m. Commercial immersion oils as Cargille RI fluids go from 1.460 to 1.640 with difference of 0.002 giving a wide range of values for experimentation [13]

$$T = \frac{4 n_s n_m}{(n_s + n_m)^2} \tag{12}$$

Different fit curves as Gaussian, Lorentzial, polynomial can be used to estimate the shape of the transmission spectra. The experimental results for PVDF films with high-roughness surface are shown in Fig. 13 for the IM method. At maximum transmission, the best RI match is found. In this case, a quartz with high-roughness was used as specimen of investigation and the deviation from the real RI value was of 0.0014 for Lorentzial fit. Polynomial and Gaussian fit have presented a 0.0055 deviation for this sample. However, the RI at maximum transmission n_{Tmax} obtained with the three fitting methods were close together and different at maximum by only 0.002. The n_{Tmax} values for a fit model depend only moderately on the set of liquids used [13].

An interpolation with different liquids over and above of n_{Tmax} can be computed. The mentioned work showed that we can obtain values of RI within an accuracy of 0.010 under the condition of at least one of the RI of the immersion liquids is substantially lower and one at least 0.05 higher than the material investigated [13]. These methods gives a simplified model to retrieve the RI of a material with irregular surface.

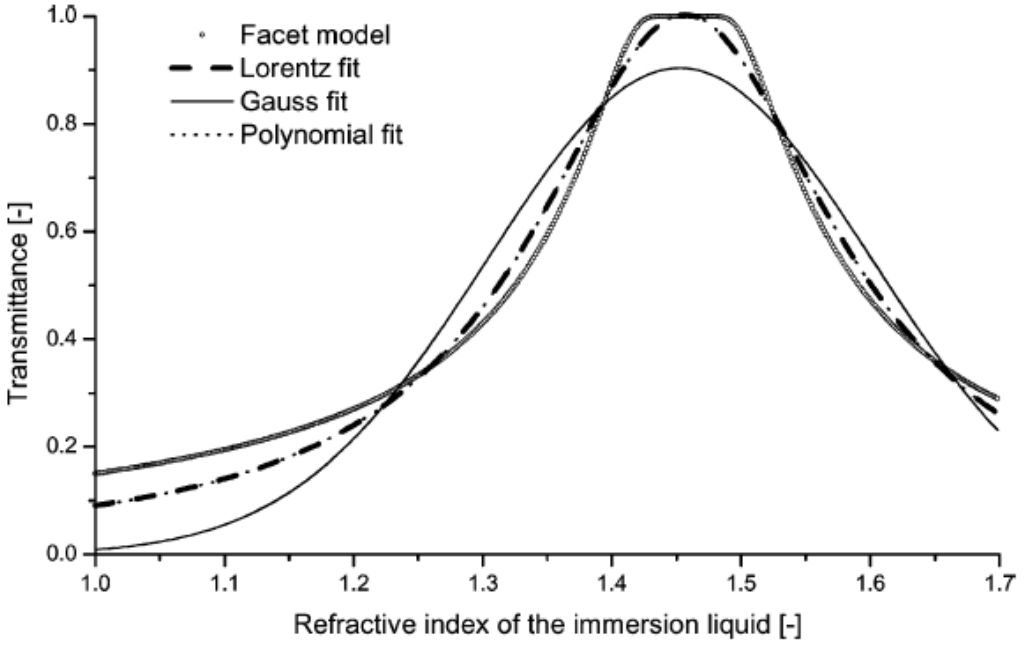

Fig. 13 Transmission of light for a high roughness surface with different models fits [13].

The presented work shows an improvement in the methodology by approximating the precise value of RI using different fitting curve models. The different model will differ at the calculation of the different position of the maximum transmission corresponding to the RI. Beside this method being model dependent, this approach increases the accuracy of the results along with the RI oils. The method overcome the limitation in dimension and shows to be suitable for complex 3D structures samples.

1.4 Comparison of Refractive Index Measurements Methods

Different methods for the measurement of RI has been presented. The characteristics of the material differ depending on the method used to obtain its physical and optical properties. By interferometry technique, sensitivity up to 0.0010 can be reach but the investigated sample require a particular shape, in the form of a two-dimensional prism, that allows to measure the difference in the interference patter from the material and a reference [6]. The sensibility of the alignment could represent a limitation since interferometric techniques have high sensibility to ambience conditions. By other hand, reflectrometry technique requires a prism with know RI as reference material in order to perform the measurements. A film in order of few millimeters on thickness has to be attached to the prism by optical bounding. The accuracy reached is up to 5×10^{-4} but limits the sample to a two-dimensional structure [12]. A similar method that requires a prism with known RI is m-line technique. By taking advantage of total internal reflection conditions strong coupling can be detected by the evanescent waves in the air layer between the specimen and the prism.

Particular RI profiles of inhomogeneous layers or multilayer systems can be measured by this technique with accuracy of around ± 0.0005 by commercial devices. The main limitation is the requirement of a minimum thickness of the sample that allows it to support the coupled modes and the air layer between the prism and the sample has to be take into account for precise results [21]. The most common commercial device used for RI measurements and other optical characteristic of materials is based on ellipsometry technique. This method allows to measure thickness and complex RI of single or multilayer up to several micrometers by polarization measurements. This technique is superior to refractometry in means of analysis of anisotropic materials providing high accuracy in the values of the RI [10].

Technique	Dimension	Size	Accuracy
Coupler m-lines	2D	hundreds of nm	0.0005
Ellipsometry	2D	few Å to several μm	0.001
Reflectrometry	2.5D	around 2 mm	0.00005
Interferometry	2.5D	few μm	0.0010
Index-matching	2D/2.5D/3D	from μm to cm	0.010

Table. 1 Comparison of different RI measurements methods with their limitations in sample dimension and size.

The main characteristic of the methods mentioned above are that the measurement of RI can be only performed in a 2D material from few Å to some millimeters depending on the technique. This is an important restriction in the geometry of the micro structures and limits the shapes of the specimens that can be measure. For this reason, we propose in this work to perform RI measurements of complex structures fabricated by TPL using the IM method. This technique has been demonstrated previously for quartz glass, crown glass and PVDF solids. It is of our knowledge that this method has not been used for the measurement of complex three-dimensional micro structures. Different oils liquids with known RI are needed where the sample is immersed and transmission values by spectrometer are performed. And in order to reduce the number of oils needed, fitting models for transmission spectral helps to retrieve the precise value of RI simplifying the experiment. Interpolation of the maximum transmission of light through a solid immersed in liquids of various refractive indices is a suited method for the determination of the RI of materials with irregular surfaces with an high accuracy. This models drastically reduces the number of experimental measurements requiring only few values of transmission to recreate the curve and find a maximum [13]. For this reason we believe this method is suitable for the performance of RI measurements for complex three-dimensional structures fabricated by TPL.

By taking advantage of the optical properties of microlenses, the calculation of effective RI measurements can be perform. By applying a reverse engineering approach, the experimental values of the focal length of microlenses can be used to calculate the effective RI of the structures. The accuracy of the method will depend on the experimental optical setup where the linear stages can scan the intensity distribution along the beam direction until finding the position of the smallest waist beam. This approach will provide a direct value of fabricated microlenses by TPL and the experimental effective RI for each structure [17]. This method will be explain in the Sec. 2.4 in a more detailed manner.

2 Experimental Methods

2.1 Sample preparation

A prior cleaning process is performed to the glass coverslit, with $n_{\text{glass}} = 1.52$, by following a standard procedure in three steps. The first step of cleaning is 10 min bath in a mix of soap and water in ultrasonic cleaner equipment. Followed by a 15 min bath of deionized water and air dry to prepare it for the final stage of 15 min isopropyl alcohol bath and finished by air dry.

An hybrid organic-inorganic photoresin SZ2080™ was used for the fabrication of the microstructures due to the high transparency in the VIS and NIR ranges and its low shrinkage of the material during the chemical development and its mechanical and chemical stability [18]. The SZ2080™ prepolymer RI was reported to be close to glass as $\sim 1.504 \pm 0.005$ at 1550 nm and 1.52 at 589.3 nm [27]. The polymer is photosensitized with 1 wt% concentration of Irgacure 369 (2-benzyl-2-(dimethylamino)-4'-morpholinobutyrophenone) to enhance the polymerization reaction [1].

The sol-gel photopolymer was drop-casted on a coverslit with 130 - 170 μm of thickness and drying on a hot plate at three stages: (1) 5 min to reach 40°C and staying 10 min, (2) 5 min to reach 70° C and staying 10 min (3) 5 min to reach 90° C and staying 40 min. The temperature gradually increases to ensure the prepolymer to acquire a uniform hard gel form. The samples were developed overnight in 4-methyl-2-pentanone after the fabrication process to remove non polymerized material and leaving the self-standing structures attached to the surface of the glass substrate. The sample was later leaving to dry at room temperature.

2.2 Laser Direct Writing Systems

2.2.1 Laser Nanofactory System

The laser direct writing of the prisms was performed by the Laser Nanofactory system from Femtika. The main element of the DLW machine is the femtosecond laser source. The laser work in a central wavelength λ_c of 1035 nm ±10 nm of high quality factor beam $M^2 < 1.2$. The laser generates pulse duration tunable 290 fs - 10 ps with pulse repetition rate of ∼76 MHz with maximum average power of 4 W at the fundamental harmonic. The experiments in this work were performed using the second harmonic λ_{sh} at 517 nm ±10 nm with 144 fs pulse duration. For the translation of the sample, the system includes a positioning system of linear stages with accuracy of ±300 nm in XY axis and ±270 nm in Z axis with maximum speed of 350 mm/s and 200 mm/s respectively. Galvano scanners are used for laser beam positioning with accuracy of 50 μrad and feedback resolution of 0.007 μrad. The fabrication process is monitoring by an integrated vision system and it is controlled by 3DPoli software. A Plan Apochromat Zeiss

63x, 1.4 NA immersion oil objective lens is used to focus the laser beam in the photopolymer. An oil immersion Immersol™ 518 Fwith $n_{\text{oil}} = 1.518$ $(23°C)$ is used between the specimen and the microscope objective, over the glass coverslit. The fabrication process is described in the cited work [16].

2.2.2 FemtoLAB by Workshop of Photonics

The laser writing of the micro optics was achieved by a customized-built LDW setup shown in Fig. 14 adapted from FemtoLAB. The following information was described from the Micro and nanofabrication technologies laboratory work. The photoexposure is provided by a femtosecond Yb:KGW laser (Pharos, Light Conversion, Co., Ldt) with central wavelength λ_c of 1030 nm, pulse duration of 300 fs and repetition rate of 200 kHz. The second harmonic was used for the fabrication of the micro optical elements at λ_{SH} 515 nm. The power converter is divided in two parts: a half-wave plate with manual rotation and a Brewster angle polarizer for an approximate maximal power and a computer-controlled rotator controlling a half-wave plate and a Brewster angle polarizer for power adjustment during the fabrication process. An immersion oil microscope lens (A-Plan, Carl Zeiss) with NA of 1.4 and magnification of 63x was used to tightly focused the laser beam into the polymer to induce the photopolymerization process. A 2x magnifying telescope ensures that the beam fills the aperture of the objective lens. A diode light source provides the illumination for the imaging live system with a CMOS camera monitoring the fabrication process by the wxPropView software. Positioning tables ANT130-110 (Aerotech, USA) with linear motor drivers translate the sample in the xy-plane while the translation of the objective lens in the z-direction is controlled by ANT130-60 positioning table. The complete system is controlled by the package of 3DPoli (Femtika, Lithuania).

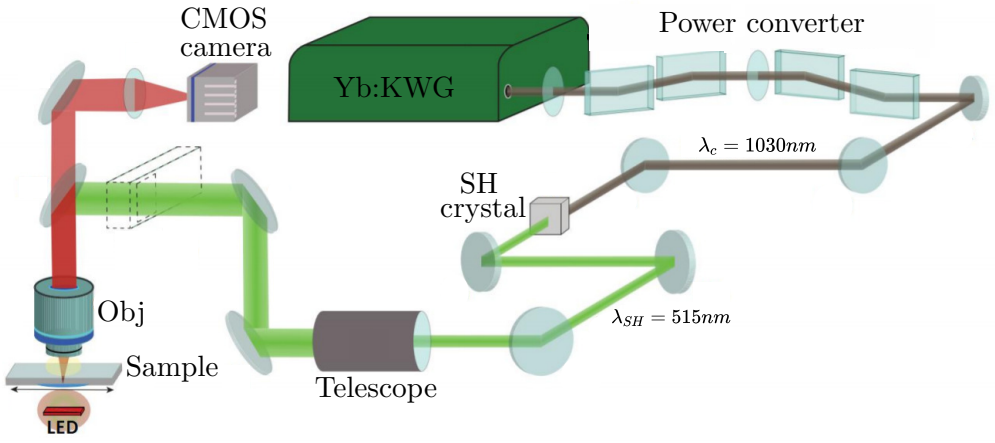

Fig. 14 Custom setup for LDW by TPL. An imaging system provides a live view of the fabrication.

2.3 Index-Matching Method Setup

The index-matching oil method was implemented to perform the RI measurements of the fabricated cuboid micro structures by two-photon lithography. A supercontinuum laser from VIS to IR (350-1750 nm) SuperK EXU3 and by filtering specific frequencies, monochromatic light was employed for illumination and a total of 17 wavelengths were used as a light source for the experiments which correspond to 450, 500, 550, 600, 650, 700, 750, 800, 900, 980, 1064, 1150, 1250, 1310, 1450, 1550, 1650 nm. Two linear polarizer control the intensity of the incidence light to ensure a fixed intensity for all frequencies employed. Cargille immersion oils worked as the RI fluids with tabulated and well reported dispersion relation and RI from 1.4 - 1.596 changing by 0.004 value. An microscope objective collects the light after the samples and directs it to a CCD camera.

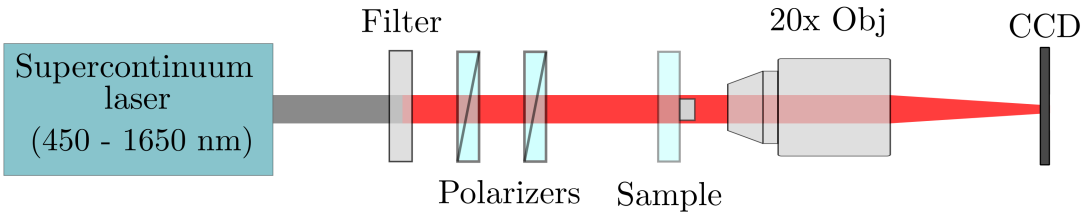

Fig. 15 Schematic of setup for immersion oil experiments. A supercontinuum laser is filtered (17 wavelengths) to obtain a monochromatic beam and the intensity is controlled by rotating two linear polarizers. An imaging system consisting in one microscope objective and a CCD camera which collects light after passing through the micro structures.

The immersed microstructures are then illuminated with different frequencies at normal incidence and the full array of elements can be illuminated at once. Due to the RI dependence on wavelength, the transmission will be different for different oils at different frequencies. The RI of the oils as function of the wavelength were obtained by the Cauchy equation.

One single structure is analyzed by cropping a selected area of the images captured by the camera. The light is transmitted and reflected at the boundary of the cuboid micro structure and the RI fluid. As the RI of the micro structure gets closer for a specific wavelength, the edges of the micro structure seems transparent having a peak of maximum intensity that is shown as the transmission of light T_1 at the closer matching RI fluid for an specific frequency. A transmission value T_0 from a section were the light went through the configuration of glass and RI fluid is taken as background reference for normalization of the transmission values as shown in Fig. 16.

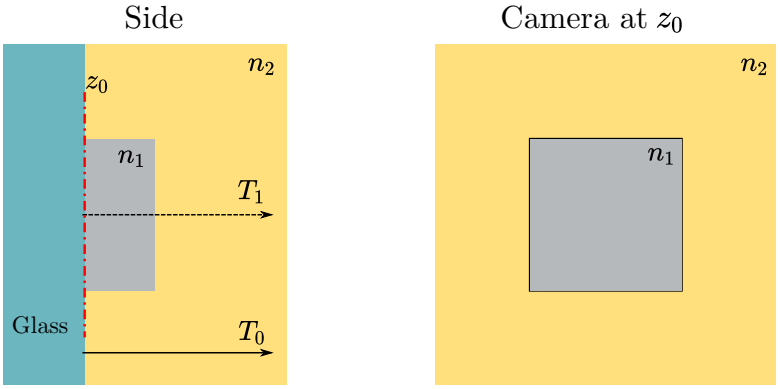

Fig. 16 Immersion oil experiment. (Left) Side view of the structures immersed in a RI liquid. (Right) Front view of the experiment. The micro structure is distinguishable when for unmatched RI between the structure and the immersion liquid.

By taking the intensity values for each oil to all the wavelengths used, a dispersion curve is built. A fitting curve of the experimental values gives the precise wavelength for a maximum transmission, i.e, intensity value. As a first approach, a Lorentzian fit as describe in Eq. 13 is used for the fitting where y_0 gives the level of the baseline, A the area under the fitted curve, A_1 and A_2 are empirical parameters that can be modified to get the best fitting, w represents the full width at half maximum and x_c and x are values related to the maximum y value [13].

$$y = y_0 + \frac{2Aw}{\pi(4(x-x_c)^2 + w^2)} \tag{13}$$

By a process of interpolation of the experimental values, for a particular oil, what frequency gives the highest intensity at the edges and the RI for that particular micro structure is found. A dispersion curve is built from the RI values at different frequencies from the IM method.

2.4 Focal Length Measurement

The fabrication of micro-optical elements by means of TPL es a field being widely studied nowadays [28]. Precise knowledge of the optical properties of the material used for the fabrication of optical elements by TPL is fundamental for an appropriate design of optical elements as are micro lenses. As a first element, a spherical lens is considered and the definition of the characteristics of the lens as it is its geometry dimensions as well as focal length can be retrieve by the Lens Maker's formula, Eq. 14 where R_2 is equal to infinite for a plano-convex lens, n_{lens} and n_0 are the RI for the lens and the surrounding medium respectively.

$$\frac{1}{f} = \frac{n_{lens} - n_0}{n_0}\left(\frac{1}{R_1} - \frac{1}{R_2}\right) \tag{14}$$

A imaging setup was built for optical characterization of micro lenses [28]. Fig. 17 shows the

characterization setup used for foal length measurements. Such setup consists in the two parts: illumination by He-Ne laser (632.8 nm) and the imaging system which contains a microscope objective lens and a camera fixed on a linear positioning stage (M-605 PI) with smaller step of 0.1 μm. A scanning along the direction of the laser beam axis provides a visualization of the spot size which at the position of minimum size is related to the focal length of the micro lens.

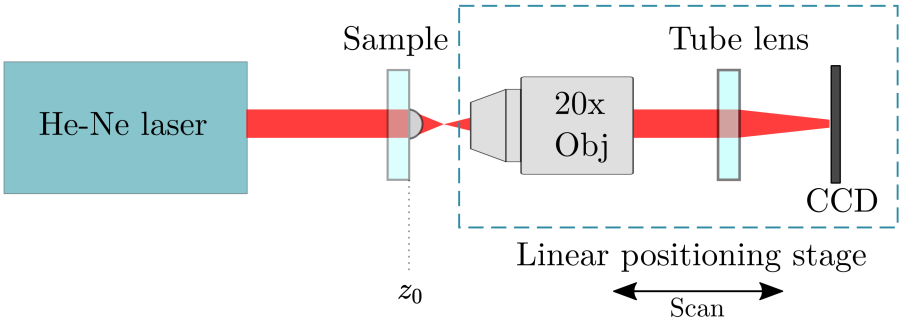

Fig. 17 Schematic of setup for focal length measurements. The sample is illuminated with a collimated beam. The imaging part of the setup is mounted in a linear stage that scans the planes along the beam direction.

The Fig. 18 shows the profile of the waist of the beam along the propagation distance. The waist is taken at the distance from the optical axis when the intensity distribution fall to $1/e^2$ fraction of its maximum value.

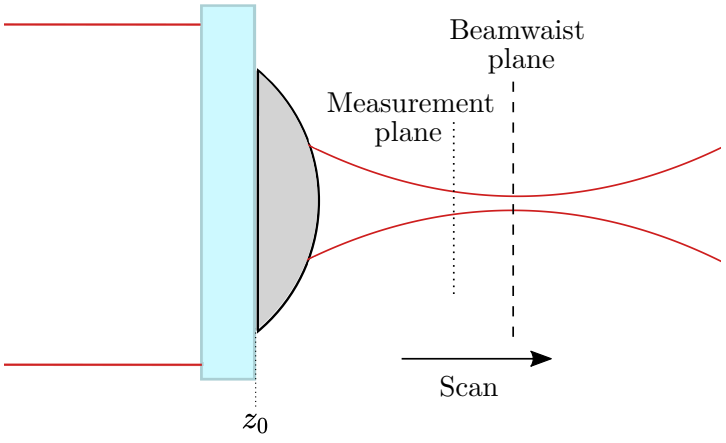

Fig. 18 Schematic of beam profile. Scan along beam propagation axis for intensity distribution measurements. Focal length found at smallest beam waits position.

The focal distance of the lens is considered at the position of the smallest waist size of the Gaussian beam. It is possible to reconstruct the profile of the beam and find the position of the smallest beam waist by scanning the planes in the beam direction and calculating the beam waist for each plane, This position corresponds to the focal plane of the micro lens.

2.5 Optical Elements Design

The versatility of TPL systems allows to write complex structures in 3D. It is well known that the roughness of optical elements has to be smaller than $\lambda/20$ to be considered suitable for optical applications [29], reason for which surface quality is of the best importance. Since optical devices are being fabricated using TPL, the understanding of optical properties of the micro structures becomes relevant. Most of the 3D geometries are a combination of basic shapes as are plane surfaces, curved surfaces and sharped edges. For this reason we focused this work in the design of cuboids and spherical lenses with known surface curvature, which fulfill such conditions. Comparison of the results for refractive indexes can be performed in means on geometry difference of the structures as well.

2.5.1 Structures Design

A cuboid was designed to measure the RI of a 3D structure with sharp edges by index-matching oil technique. The structure was created by linearly scanning layer-by-layer in order to fill up the volume of the prism. This method provides higher control over the scanning steps and the voxel overlap. This allows to achieve the surface quality expected without approaching by a more complicated scanning method. Considering an overlap of around half voxel dimension in the lateral and transverse dimension, the scanning lines were done perpendicular to previous scanning lines layer direction.

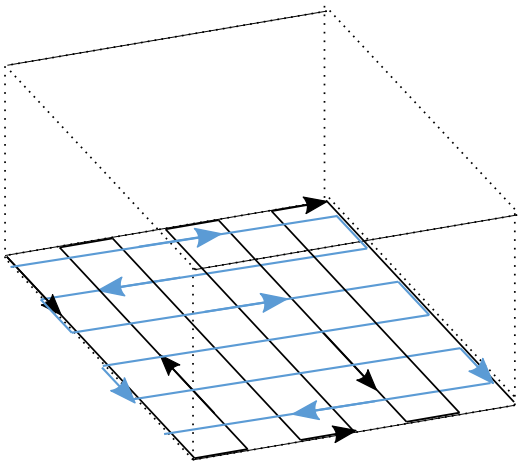

Fig. 19 Writing scanning for micro cuboids. The laser scans layer-by-layer to build up the volume of the structure. Each even layer is changing the direction creating a grid to maximize voxel overlapping.

Spherical lens where chosen for their simple design. The dimensions required for the lenses where based on the limitations of the focal length measurements and the fabrication time required for such structures. Fig. 20 shows the geometrical approach was used to obtain the

values required of radius R obtained by $R = H/2 + D^2/(8H)$, for a fixed diameter D and different values of thickness H. For different values of R and H will give different focal length is expected as described in Eq. 14.

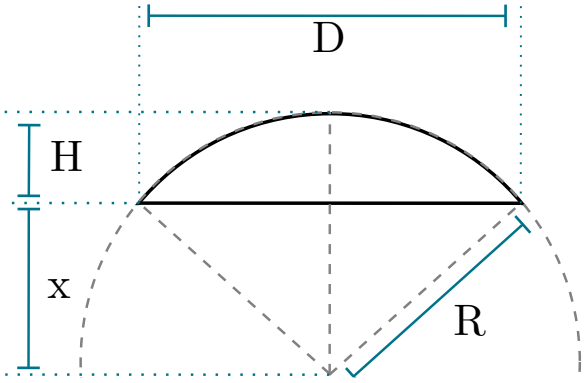

Fig. 20 Geometrical relation between a desired diameter D of a spherical lens, thickness H and radius of curvature R.

In order to obtain a smooth-shaped micro spherical lens with surface quality suitable for optical applications, different scanning modes has been previously presented for lenses fabricated by TPL. Approaches to fabricate the spherical lens have been done by using parallel linear scanning, fixed constant delta Z and annular scanning mode with constant delta Z, distance between layers, and dynamical Z [30] as well as subregional slicing methods [31] and equal-arc slicing [3] for curved surfaces. Results from last methods have shown an improvement in optical quality of the lenses and reduced the fabrication time but the complexity of the implementation is still a limitation. Since the structure is fabricated point-by-point we have highly control over the beam path followed to get TPP in the material. The overlapping of voxel in both, lateral and transverse directions, determines the lens quality and surface smoothness.

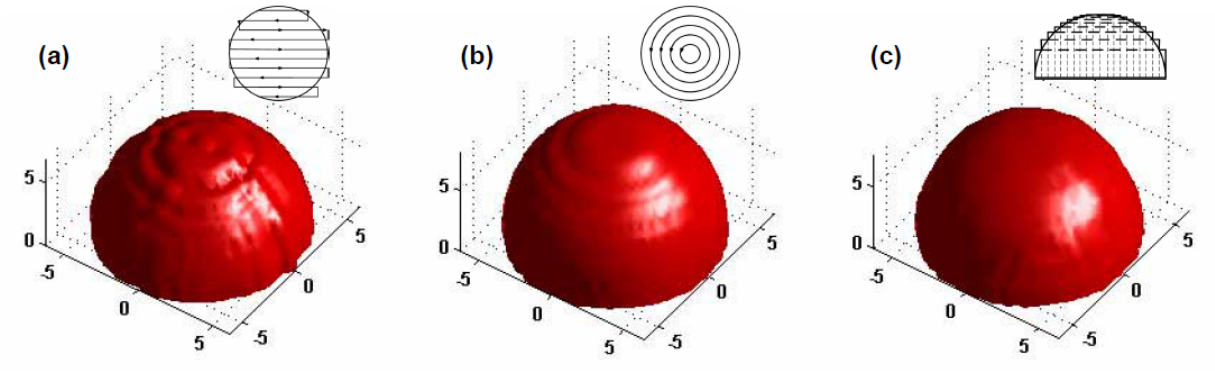

Fig. 21 Simulations of micro fabrication scanning modes effects on lens surface quality. a) Parallel linear scanning with fixed Δ z. b) Annular scanning method with fixed constant Δ Z. c) Annular scanning method with dynamical Z [30].

Two different approaches where implemented for the design of the spherical lenses. The use of linear writing method of spherical structure do not provide the quality required for micro optics. In order to overcome this problem we proposed two different writing methods where the curvature of the structures is taken into account in the writing process.

2.5.2 Spiral Sphere Writing Method

An spiral concentric path was implemented for the beam during fabrication to obtain a better quality on the surface of the spherical lens. The route followed by the beam is determined by Eqs. 15 which give the position in Cartesian coordinates coordinates map spirals over a sphere with constant increasing radius form a 3D spherical shells. The coordinates evolve from zero to $a_{\max}$ which is the value of the radius. Such results come from the parametrization in Cartesian representation of the 2D Archimedian spiral in polar coordinates $r = f(\phi) = a\phi$ where the radius r is defined by the increment multiplier a and the angle ϕ [32]. The Fig. 22 shows the outer shell layer of the spherical lens described by an spiral path.

$$
\begin{aligned}
x = f(a) &= r\cos(a)\cos\left(\frac{-\pi}{2} + \frac{a}{a_{\max}}\pi\right) \\
y = f(a) &= r\sin(a)\cos\left(\frac{-\pi}{2} + \frac{a}{a_{\max}}\pi\right) \\
z = f(a) &= -r\sin\left(\frac{-\pi}{2} + \frac{a}{a_{\max}}\pi\right)
\end{aligned}
\tag{15}
$$

2.5.3 Circular Writing Method

The spherical lens is created point by point of the polymerized material created by the path followed by he beam withing the prepolymer. This path is defined by concentric circles, defined by Eq. 16, in the Circular writing method. The slicing of the lens is done vertically by

defined the z position, changing by a relation to $dR_z = 0.5\ \mu\text{m}$. While the difference in distance between the circles in the same z-plane was constant by $dR_{xy} = 0.1\ \mu\text{m}$.

$$\begin{aligned} z &= \sqrt{R - dR_z} \\ x &= \cos(\alpha) \\ y &= \sin(\alpha) \end{aligned} \tag{16}$$

$d_z = \sqrt{R_{max} - R}$ for an R going from 0 to R_{max} with a delta of $dR = 0.5\ \mu\text{m}$. These circles are defined from the center of the lens at the interface with the glass coverslit, at $z = 0$, to the radius of the lens represented as R_{max}. A step of $d_{xy} = 0.2\ \mu m$ is considered in the with different radius with distance of 0.5 μm between each other as shown in Fig. 22. The equations define the position of the beam in Cartesian coordinates by the circle equation from Eq. 16. The angle controls the writing distance from one point to another in the xy-plane.

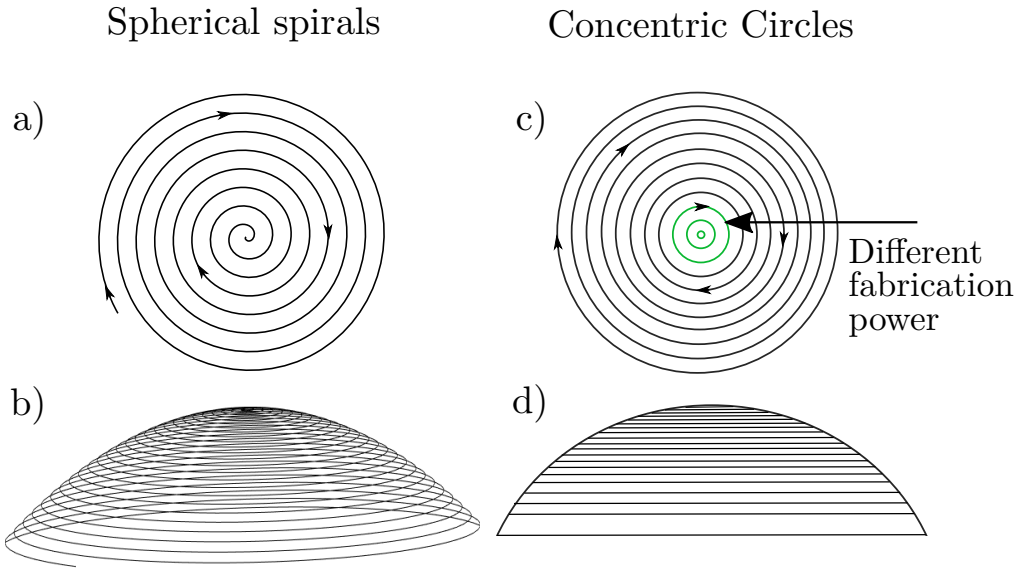

Fig. 22 Writing methodologies for fabrication of spherical micro lenses. Spiral sphere method a)upper view and b) side view of spherical shell. Concentric circle method c) upper view showing a change of the fabrication power at the center and d) side view of the fabricated layers.

This configuration provides high control over the geometrical and writing parameters as are the angle between single points that create the individual circles, the distance between circles, the distance between layers and the fabrication power of each individual circle. In comparison with the Spiral writing method, this method provides a straightforward control over the geometric parameters and less computational time required for the generation of the beam path that creates the spherical lens.

3 Results

The RI of the material changes after the polymerization process. As mentioned in the Sec.1.3, several research has been performed for the understanding of the RI of different materials after the polymerization process being focused on thin films polymerized by UV light. A droplet of SZ2080™ prepolymer with 1 wt% of photoiniciator was illuminated with UV radiation until a polymerization state was reached. The UV polymerized droplet is then development following the standard procedure. Lines by TPL are then inscribed in the already photopolymerized droplet by UV light. It is shown in Fig. 23 that applying TPL technique after a SPP, it is possible to keep polymerizing the material to a higher value by increasing its degree of conversion.

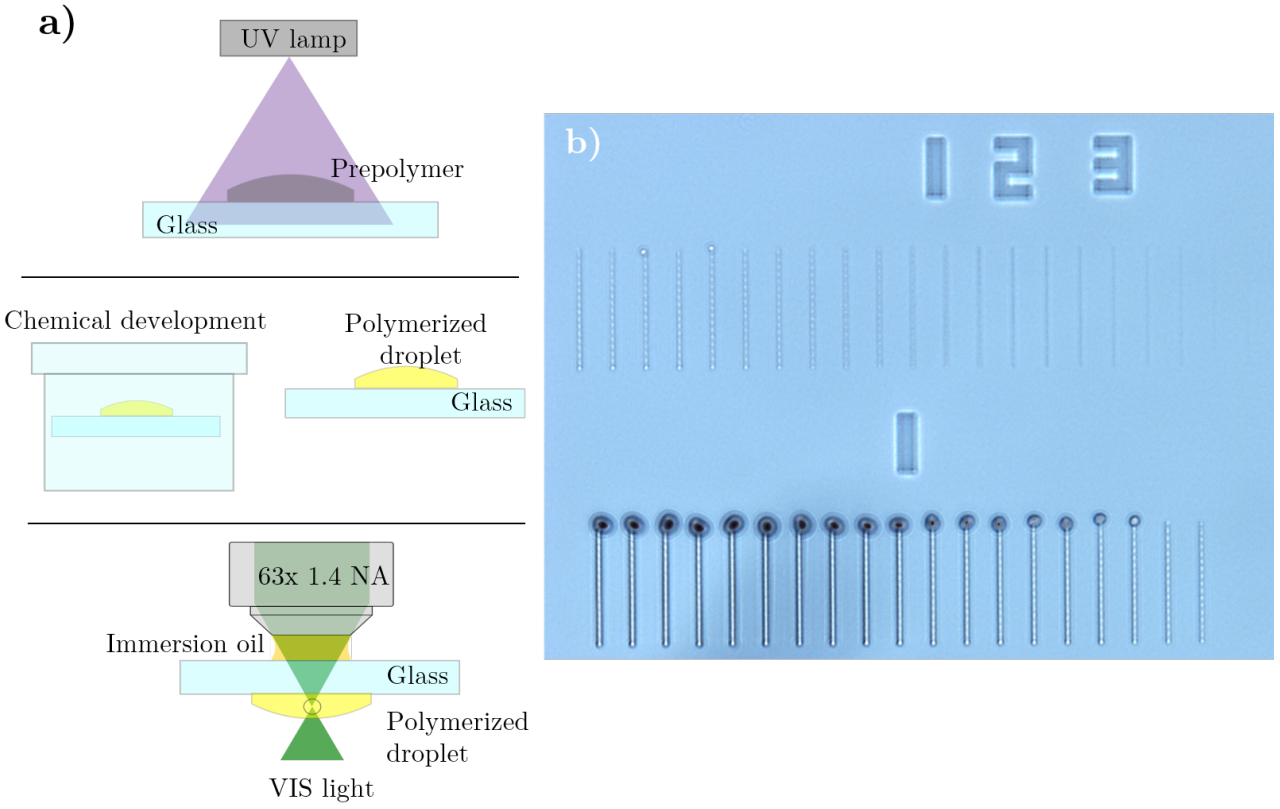

Fig. 23 a) Process of dual-curing photopolymerization: UV light illuminates the prepolymer droplet until a polymerized state is reached. The droplet is developed in a chemical bath. The UV polymerized droplet is expose to TPL to fabricate structures of higher degree of polymerization. b) Optical microscope image of lines fabricated by TPL out of a UV polymerized droplet.

To demonstrate the difference, resolution bridges were fabricated in fresh prepolymer by only using TPL. The Fig. 24 shows the optical image showing the transparency of the elements as well as the Scanning electron microscope (SEM) image of high magnification of the fabricated lines from where the dimensions can be obtained.

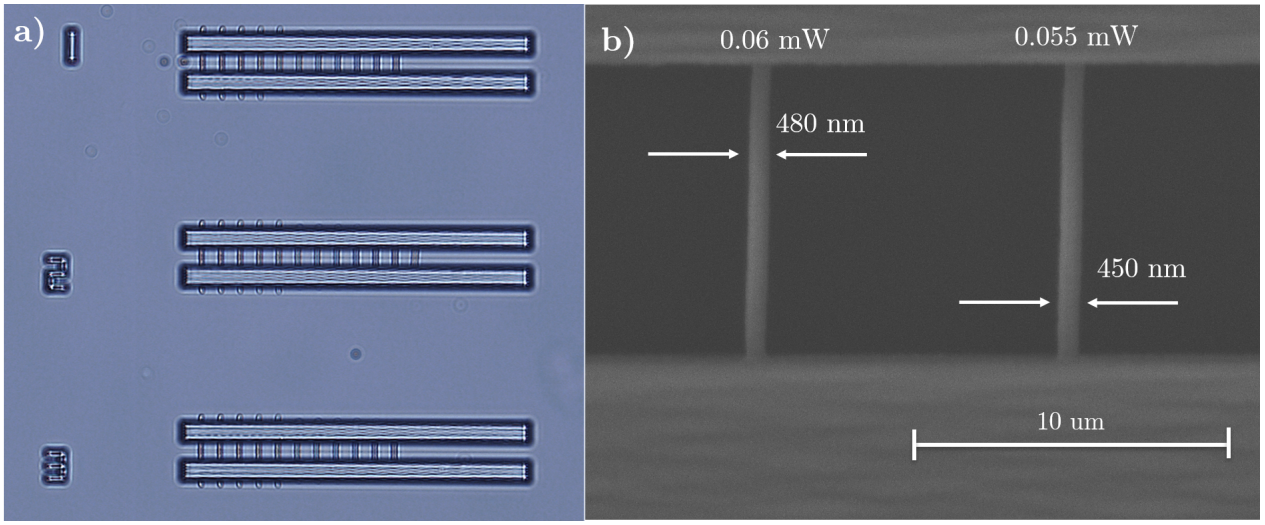

Fig. 24 a) Optical microscope image of resolution bridges for voxel dimension measurements. b) SEM images of high magnification of two lines with fabrication power 0.06 and 0.055 mW are shown with corresponding d_{xy} voxel dimension.

The fabrication window includes the parameters needed for structuring the material. Keeping all the experimental variables fixed including the writing speed as 500 μm/s, then it can be defined by the empirically determined intensity range, between irreversible polymerization and optical damage in the material. Different power values mW where employed for the writing of the lines show in Fig. 23. From the test realized for single lines in the prepolymer solution, it is found that lower powers result in an unwashed polymerizated lines after UV exposure than for a direct TPP fabrication within clean prepolymer.

3.1 Microcuboids

The cuboids micro structures were fabricated using the Nanofactory System with a theoretical line volume of 48.56 μm^3 for a writing speed of 500 μm/s. Five different writing power were used, in the range of 2 to 4 mW, for the fabrication of the micro cuboids of 8 μm of height and 16 μm of length. The Fig. 25 shows the resulting structures by a Scanning Electron Microscope (SEM).

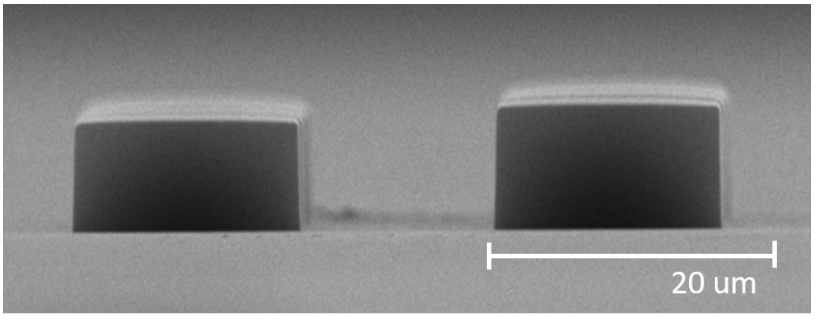

Fig. 25 SEM images of micro cuboids of 16μm length and 8 μm height for RI measurements.

The experimental overlapping calculated varies according to the fabrication writing power. The theoretical voxel overlap under such conditions is around 50% considering and axial displacement of 0.16 μm and 0.32 μm for longitudinal displacement.

For the implementation of IM method, 60 arrays of 5 microcuboids with different exposure dose were fabricated since each array was measure with a different RI oils. A writing speed of 500 μm/s was kept constant for the fabrication of all the elements of all arrays. The fabrication laser powers used were in the range of 2 to 4 mW.

3.2 Results IM method

In order to retrieve the RI of the cuboids micro structures, the methodology presented in Sec. 2.3 was implemented. For each wavelength used for illumination of the samples, a RI was retrieve for each of the writing power used. The RI were obtained by a Lorentzian fit [13] where the level of distribution, the amplitude and the resonance waist was adjusted for the data. The RI values that correspond to the best matching with the RI oil for each wavelength was taken where the amplitude of the resonance was maximum. This method was implemented for all wavelengths used and all structures of different powers.

The Fig. 26 shows an exemplification of the index-matching oil method of a sample array of micro elements fabricated by TPL immersed in a RI liquid Immersol™ 518F and imaged by optical microscope (Olympus BX51) in reflection mode. As shown in the image, by immersing the micro structures in an liquid with close RI value of the one of the micro structures, they seem to be transparent for an specific illumination wavelength.

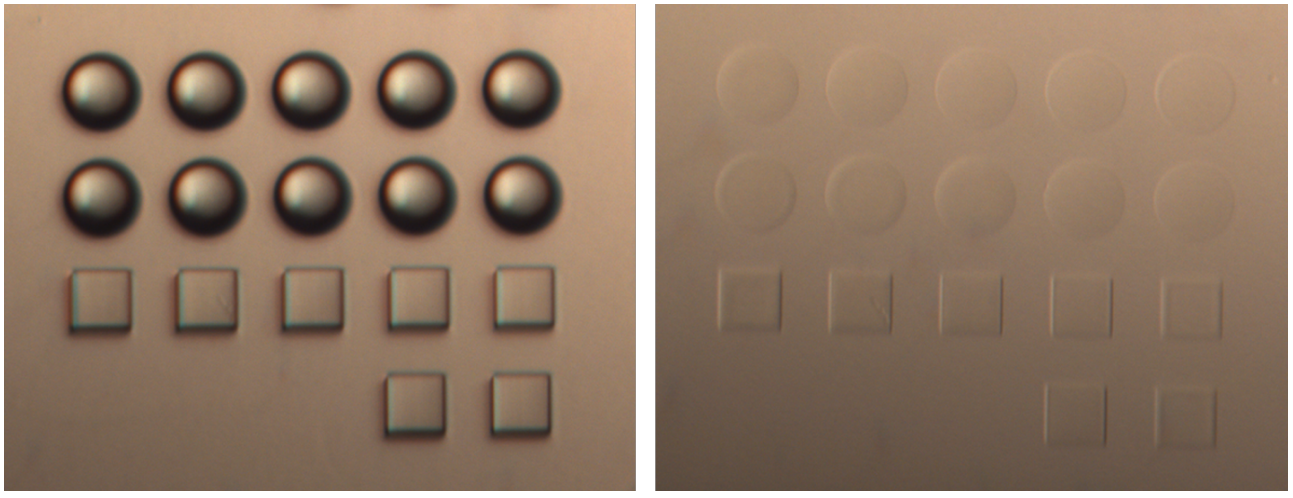

Fig. 26 Index-matching oil experiment. An array of micro elements is immersed in a liquid of $n = 1.518$ showing that the transmission increases by approaching RI matching.

From the obtained values of RI for all wavelengths a dispersion curve was built and the

parameters A, B and C were obtained by adjusting the Cauchy equation. These values varies depending the seed value used for the adjustment but the shape of the curve keeps remains. The Fig. 27 shows the values of the RI for wavelengths on the VIS - IR range. Five different values of writing power were used from 2 to 4 mW for the fabrication of the cuboids with same geometrical dimensions.

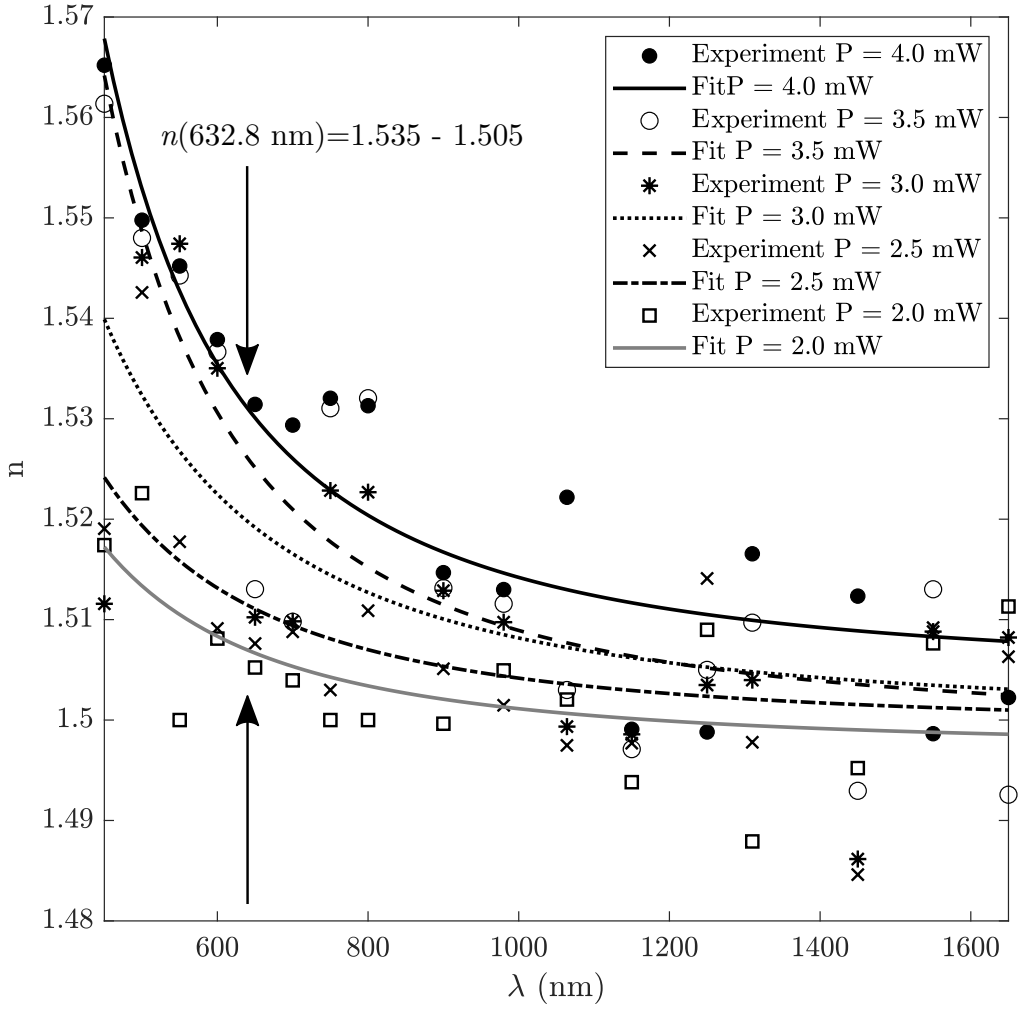

Fig. 27 Results of RI. The power used for fabrication was in the range from 2 to 4 mW.

3.3 Spherical lens

The spherical lenses were fabricated following the previously mentioned methods in Sec. 2.5.1 by the FemtoLAB by Workshop of Photonics system. As a first approximation, the Spiral sphere writing method was employed. For this, an additional parameter that controls the number of spirals was added to the Eq. 15 in order to keep the same distance between spirals for different lens' radius. The Fig. 28 shows the resulted fabrication of lenses of 50 μm diameter and 5 μm of thickness from both writing methods. As shown in the SEM images, some defects on the lenses resulted from such methodologies. From the Spiral writing method the lenses

were burnt at the center due to the high overlapping of the voxels. In order to get rid of this defect at the center, a reduction of the spirals at the center of the lens was applied resulting as a hole at the center of the structure. Another defect presented close to the edges of the lens was due to the circular motion of the laser during the fabrication process to create the spirals.

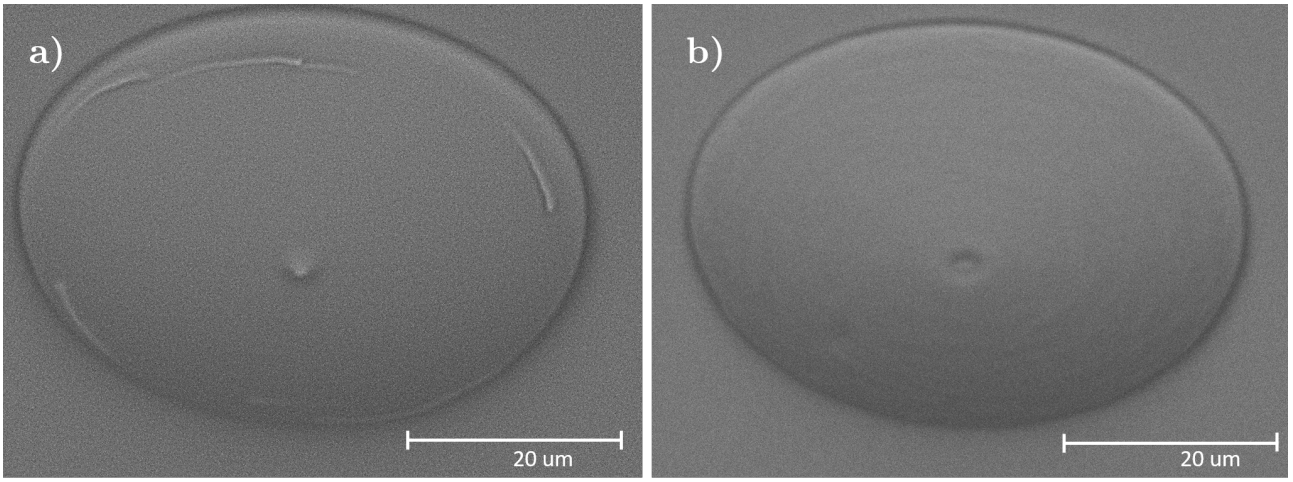

Fig. 28 SEM images of spherical micro lenses of 50 μm of diameter and 5 μm of thickness by two different writing methods. a) Spiral sphere method resulting in defects at the edges and the center of the lens. b) Concentric circles writing method by adjusting the exposure dose at the center of the lens to avoid defects.

In order to have a higher control under the writing parameters, the Circular writing method was implemented. This method allows to have control in the distance between circles at the center of the lens as well as in the fabrication power of each circle. As shown in Fig. 22 c), a reduction of the power by 10% in the circles under 1 μm at the center was implemented in order to avoid burning by thermal accumulation. Part of the uniform surface is improved due to self-smoothing and non-local polymerization effects caused by the material properties.

As final structures, we fabricated three lenses of 75 μm diameter and 5 μm of thickness close to each other at constant writing speed 500 μm/s for the three cases. Three different writing powers were consider for the fabrication: 0.06 mW, 0.05 mW and 0.04 mW named as high, medium and low dose in the following part of the document, and considering a experimental voxel value of 0.5 μm. The Fig. 29 shows a SEM image of such array of micro lens where the surface at the center of the lens was improved.

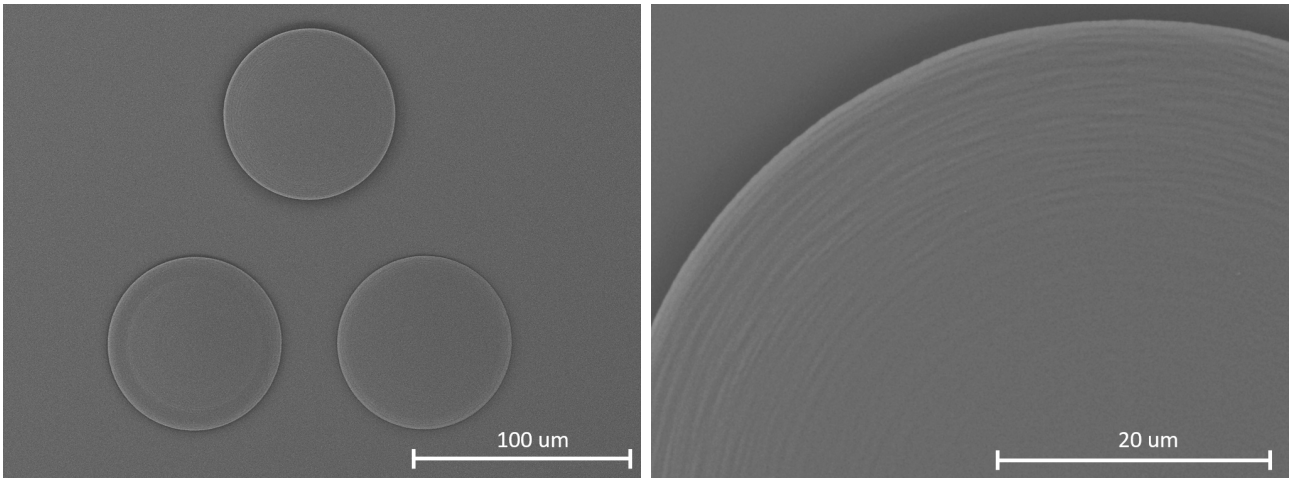

Fig. 29 SEM images of an array of spherical micro lenses with a diameter of 75 μm. (Left) Array of 3 spherical micro lenses with different exposure dose and same geometrical dimensions. b) Surface of micro lens fabricated by Concentric circles writing method.

The samples where covered by a thin layer of around 20 nm of Ag for SEM and profilometer measurements. The geometrical values of the fabricated micro lenses were obtained by profilometer measurements (Sensofar PLu 2300) and microscope objective of 100x magnification where we found with a good accuracy with the designed dimensions as shown in Fig. 30. The results for the experimental values of dimensions are shown in Table. 2

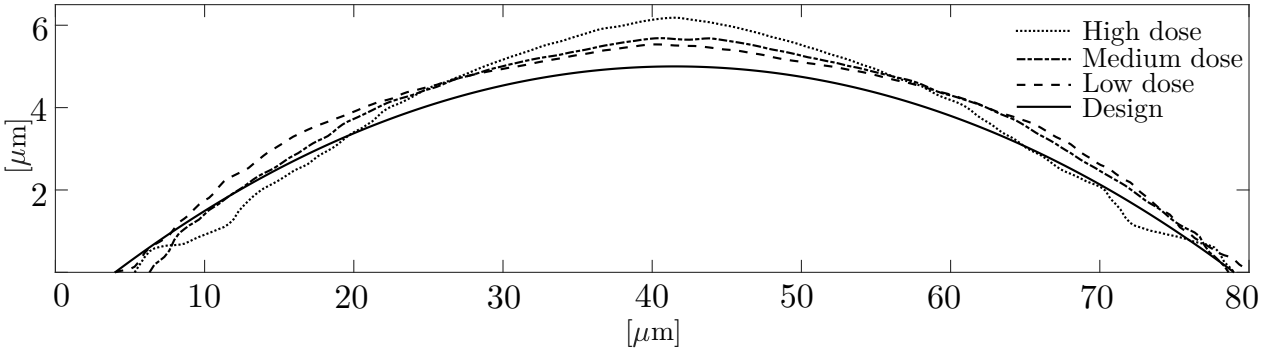

Fig. 30 Profilometer results of micro lenses. Comparison with design profile of spherical lens and experimental values.

Lens characteristics	Diameter μm	Thickness μm	Deviation D	Deviation H
High dose	73.7	6.2	23%	1.7%
Medium dose	72.4	5.7	14%	3.4%
Low dose	75.7	5.5	10%	0.9%

Table. 2 Experimental dimension values for array of three lenses and deviation from a virtual lens of 75 μm and 5 μm thickness.

3.4 Characterization of optical performance

3.4.1 Imaging performance

We proved the optical performance of the array of micro lenses showed in Fig. 29 by imaging a Target unit (Thorlabs R3L1S4P - Positive 1951 USAF) in a optical microscope configuration (Olympus BX51). The target unit was placed at infinity, i.e, at some distance from the micro lenses and illuminated by white light. Different planes where imaged by a 40x microscope objective and translating the sample with a micrometer translator in the optical microscope.

The Fig. 31 a) shows the interface plane of the sample, the boundary between the glass cover slit and the plane side of the micro lenses. By translating the sample, we found that the lenses have different focal length as expected. The Fig. 31 b)-d) show the imaging performance of the spherical lenses at each focal plane. The micro lenses were fabricated with three different fabrication powers named high dose for 0.06 **mw**, medium dose for 0.05 **mW** and low dose for 0.04 **mW**. We can see from Fig. 32 that the lenses are capable of image the smallaest group from the target used.

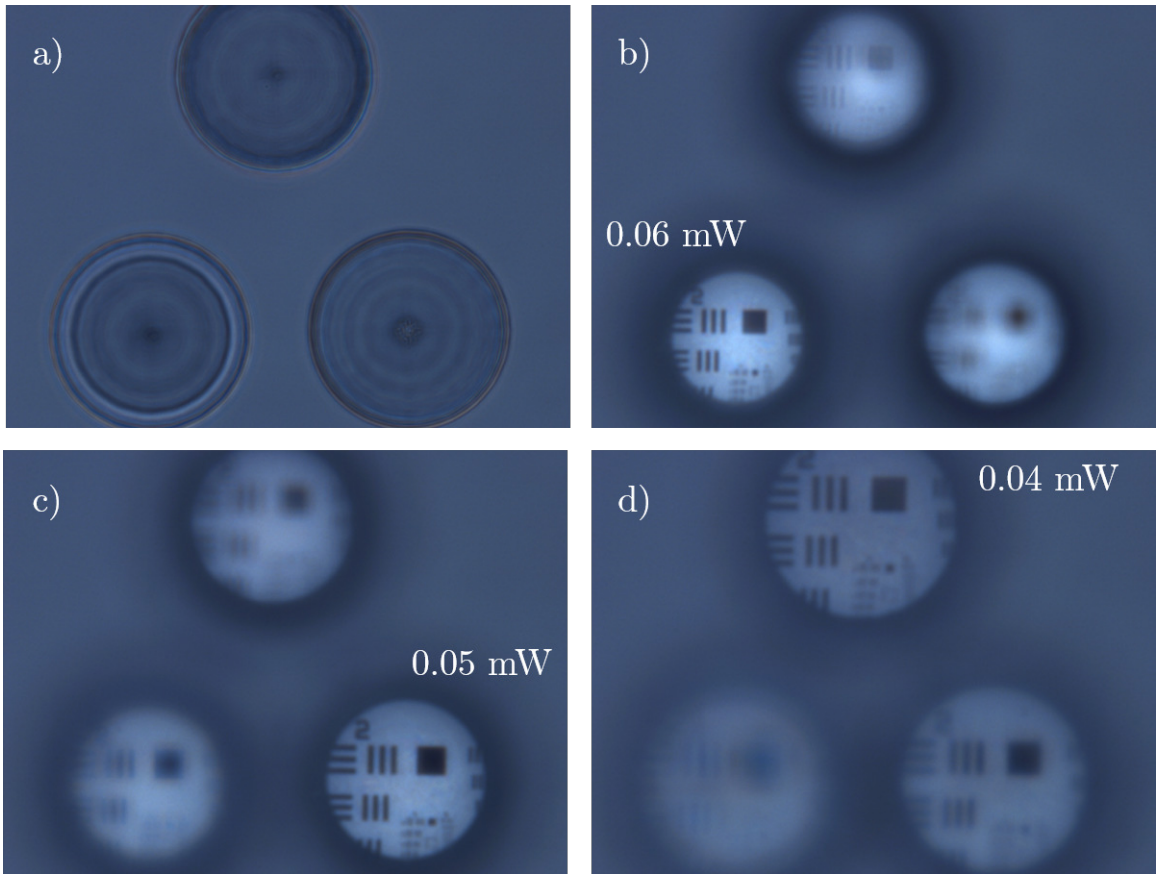

Fig. 31 Optical microscope images of array of micro lenses. a) Interface plane, the lef bottom lens shows defects after the fabrication, b) - d) focal plane of lenses of different fabrication radiation power.

The micro lenses are capable of imaging a clear target image at their focal plane proving their optical performance as shown in Fig. 32. The qualitative results from the imaging of the lenses by the optical microscope prove the dependence on writing power fabrication in the RI of the micro structures.

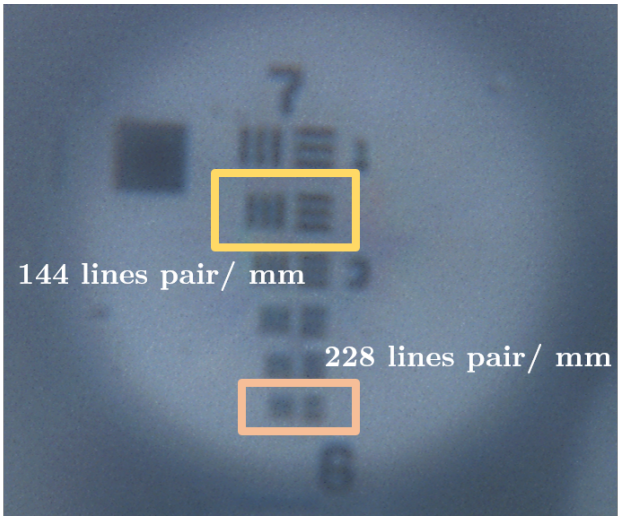

Fig. 32 Optical microscope images of array of micro lenses. Resolving power of 7 μm by imaging a target (Thorlabs).

The resolving power of the lenses was found by imaging the target presented. By distinguishing the lines of the target group 7 and element 2 which corresponds to 144 lines pair/mm results in a resolving power of 7 μm. From the images obtained by the lenses it is shown that the microlenses are capable of imaging and confirms their suitability to perform optical applications.

3.4.2 Focal length measurements

The methodology described in Sec. 2.4 was implemented for the measurements of the array of 3 spherical micro lenses as a quantitative method for focal length measurements. A scanning of 1 μm step along the optical axis was performed to measure the respective focal length of each spherical lens and capturing the intensity distribution of the fundamental Gaussian beam by a beam profiler (DataRay WinCamD). By retrieving the radius of the beam at $1/e^2$ value of the intensity (13.5%) we generated a profile of the Gaussian beam along the z-axis for the minor and major axis of the intensity beam distribution. The Fig. 33 shows the intensity distribution approximated to a fundamental Gaussian beam at two different z-position for one single lens of 75 μm of diameter and 5 μm of thickness. The Fig. 33 a) shows the intensity distribution of the beam at its focal distance while the Fig. 33 b) shows it for a different z-distance.

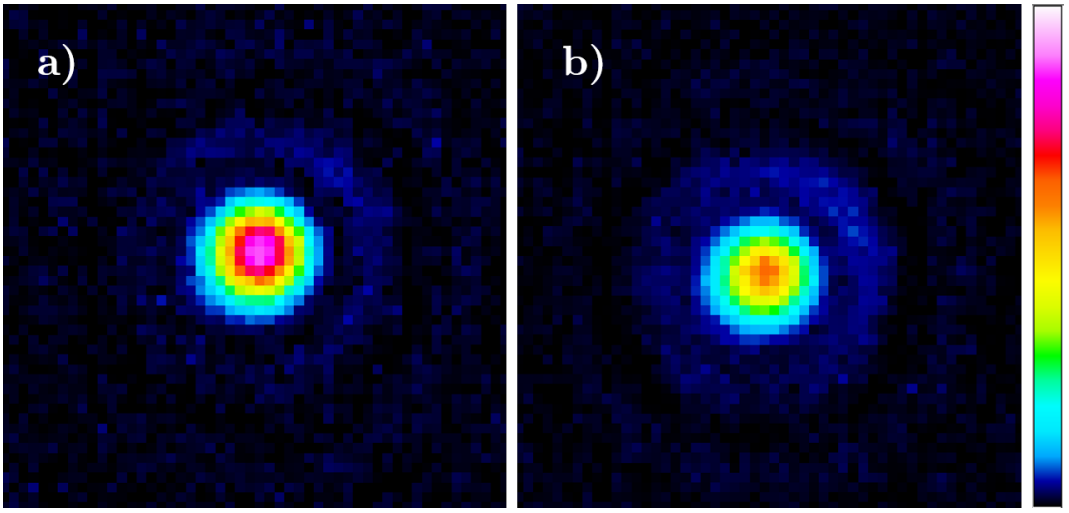

Fig. 33 Experimental intensity distribution of a He-Ne beam passing through the fabricated micro lenses. The images were collected from DataRay software showing a) focused beam at focal plane and b) image plane close to focal plane.

In order to obtain the focal length value for each lens, a scanning of the intensity distribution was performed in a range around the plane of the smaller beam waits. In the Fig. 34 we can see that the experimental values of the beam waist for different planes around the focal distance provides the shape of the beam profile as expected. A polynomial fit of 5th order was implemented to find the position corresponding to the smallest waist of the beam. From this results we can retrieve the position where the smallest beam size is positioned for both axis of the intensity beam distribution for each lens.

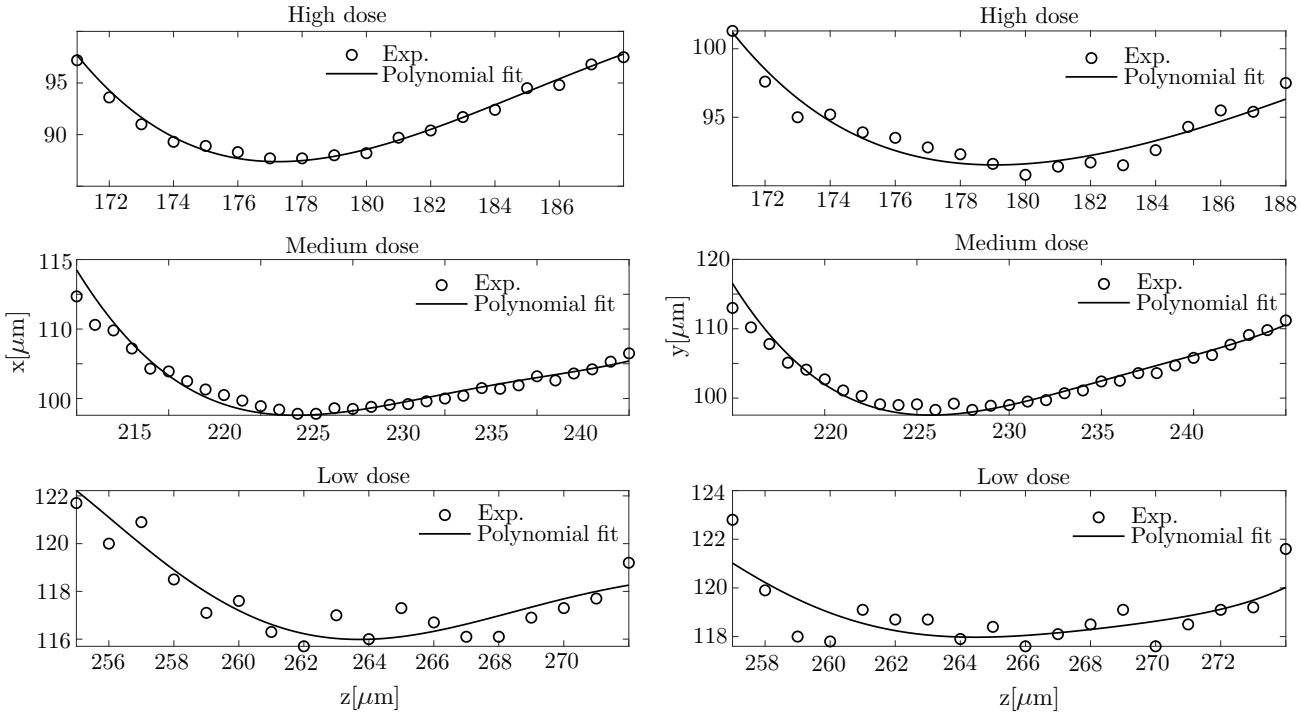

Fig. 34 Experimental values of beam waist for different z-position along beam propagation axis.

By implementing a reverse engineering approach, we retrieved the values of the RI for lenses of such geometrical dimensions by the Eq. 14. The Fig. 35 shows dependence of RI on the focal length for the fabricated micro lenses. A recalculation of the corresponding RI from the experimental values dimension of the lenses was performed and a comparison is showed from the expected relation from the design dimensions.

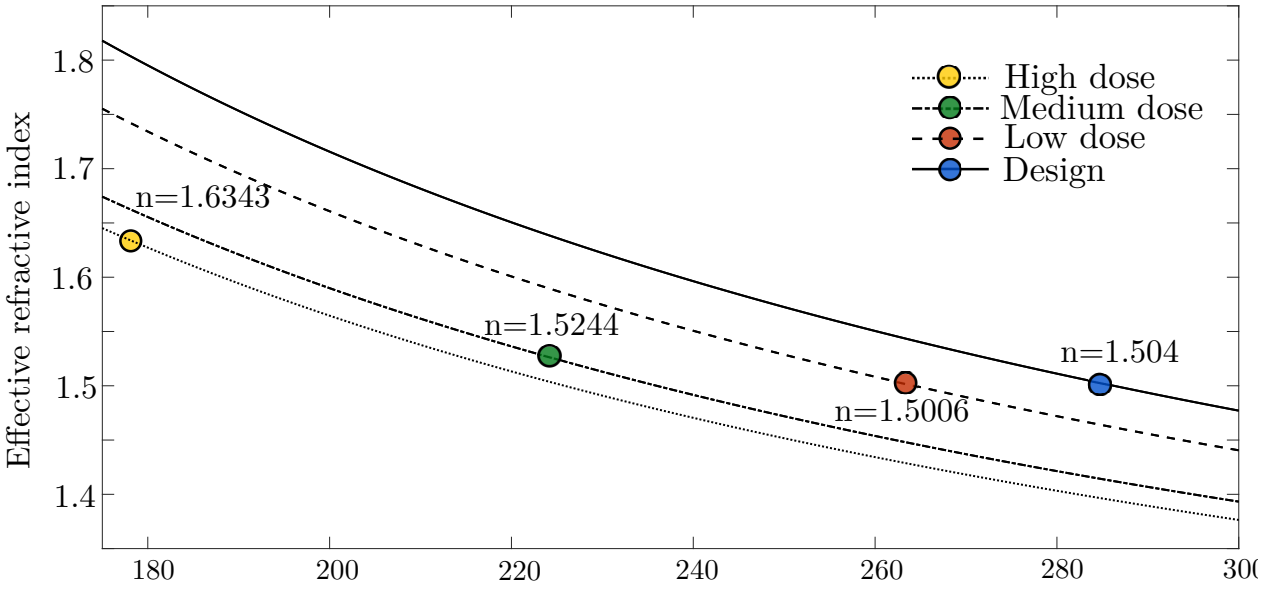

Fig. 35 Relation between focal length and the effective RI with experimental values. The expected behaviour for a virtual lens of 75 μm diameter and 5 μm thickness is shown for comparison.

The Table. 3 presents the experimental values of the focal length for each lens considering the same interface plane or plane at $z = 0$ position. Their corresponding RI value are taken from the calculated theoretical values shown in Fig. 35.

Lens characteristics	Fabrication power	Experimental f	Theoretical n
D=75 μm	0.06 mW	178±1 μm	1.6343 ± 0.004
H=5 μm	0.05 mW	225±1 μm	1.5244 ± 0.002
R=143.1 μm	0.04 mW	264±1 μm	1.5006 ± 0.002

Table. 3 Experimental focal length values for array of three lenses of 75 μm and 5 μm thickness. Theoretical RI for corresponding focal length values of micro lenses.

The expected RI values were recalculated for each lens taking into account their experimental dimensions. A shift in the values of RI is shown for experimental dimensions that are in an error range of less than 20%. The results are in the expected range from index-matching method results.

4 Discussion

Two-photon lithography is an attractive technique for the shaping of a prepolymer material by means of photopolymerization mechanisms. Due to its versatility it is being widely implemented for the fabrication of micro elements for optical applications. Such kind of elements require a precise understanding of its optical properties where the RI plays an important role. The effective RI depends on the geometry of the optical elements which could differ from the intrinsic RI of the material. In the literature, it has been presented different methodologies as are interferometry, reflectrometry, coupler m-lines and ellipsometry for the RI measurements of photopolymerized materials. The main characteristic of such techniques is the limitation in the dimension of the specimen to measure since they only accept 2D samples. Another characteristic of reported RI values is that the photopolymerization mechanisms used is single-photon lithography which polymerize the material in an homogeneous way. The results from Fig. 23 shows that it is possible to increase by TPL the degree of polymerization already previously polymerized by UV light demonstrating that reported results of RI values are not suitable for consideration after TPL. In order to overcome these limitations, a proposed methodology for 3D micro structures fabricated by TPL was proved. The index-matching oil method is suitable for 3D micro structures of complex shape.

In this work we present the fabrication of micro cuboids and micro spherical lenses by TPL for RI measurements by two different methods: index-matching oils and focal length measurements. The micro cuboids were fabricated by the layer-by-layer writing method which allows a high control in the overlapping of the voxel by around 50% by filling up the volume of the micro structure. Five different fabrication powers where used withing the range of the fabrication window corresponding an intensity range from 0.208 to 0.415 $\mathbf{TW/cm^2}$. A dispersion curve was built from the results of RI dependence of illumination wavelength for different RI liquids as immersion medium. The results presented in Fig. 27 show that different writing power used for fabrication result in different RI of the final structure. The values are in the range of the previously reported for the SZ2080™ under UV polymerization but showing the increment of the value by increasing the fabrication power. These results provides an accurate value of RI for different wavelength dependent on the fabrication parameters. Such results allows to consider a more precise approximation of the RI value which is required for micro optic elements design.

For the micro optical lenses, the first writing method used named Spiral Sphere method presented defects on the resulted micro lenses as well as long fabrication time. Besides of showing a smooth surface with sufficient quality for optical applications, the defects affected the optical performance of the lenses. To overcome this problem, we fabricated micro lenses by the Circular writing method. Such method allows a higher control in the voxel overlapping as

well as in the fabrication power for each individual circle. Due to mechanism it was possible to reduce by a 10% the power for the circles below of 1 μm radius at the center avoiding burning. By applying this methodology, we fabricated three lenses of same geometrical dimensions, 75 μm diameter and 5 μm of thickness next to each other to perform imaging and focal length measurements. Three different powers were used for the fabrication that corresponds to intensity range from 0.19 to 0.28 $\mathrm{TW/cm^2}$. The micro spherical lenses where geometrically characterized by SEM images as shown in Fig. 29. The surface quality is suitable for optical applications and beside the dimensions of the lenses being less than 20% error, the lens fabricated with the higher dose, corresponding to a 0.06 mW of fabrication power, shows surface defects that affect its optical performance. This defects are due to fabrication problems and additional samples can be fabricated in order to improve the fabrication methodology.

The spherical microlenses show its capability of imaging in Fig. 31 proving the optical quality that is sufficient for optical imaging of a target of resolving power of around 7 μm. All three lenses fabricated by different writing powers image a target unit illuminated by white light. The image plane distance is shift from one lens to another due to the difference in fabrication results as expected. By the difference in focal distance for each lens and their experimental dimensions, we proved the RI dependence on the fabrication parameters. This is confirmed by the experimental results of the focal length of the lenses. By retrieving the theoretical values corresponding to the experimental values of the focal length of the micro lenses we find the dose dependence of the RI of the elements. An experimental error has to be consider for the precise value of the RI as well as fabrication errors or defects on the lenses affect their optical performance as demonstrated in the high dose lens where the RI is out of the expected range. Besides the fabrication challenges it is demonstrated that different fabrication exposure dose for same geometrical micro =lenses results in a different optical performance due to the change in their RI value. The single lenses showed a comparable optical performance than compound structures of hundreds of μm size fabricated of TPL [9] despite that the focal length values obtained are affected by the geometrical experimental conditions.

This is a new finding since proves that the RI of elements fabricated by TPL out of SZ2080™ differs from the previously reported in literature (n=1.504 for 632.8 nm). The IM method shows the dose dependent withing the range of RI from 1.515 to below 1.6 for different illumination wavelength. The results for RI presented from both methods shows a discrepancy with the RI value of SZ2080™ of 1.504 for 632.8 nm illumination after SPP. This shows that there is an increment in the RI of the microelements fabricated by TPL.

Since this technique allows a high control on exposure dose during fabrication, the calculation of this experimental values of RI concede the possibility of design and fabrication of 4D

printing of free micro elements and components. By using the same material and one single techniques which is TPL, it will be possible to create compounds micro optical elements in a high precision manner. This will allows to replicate micro optical components out of a single material reducing the fabrication problems and increasing the flexibility in the design.

5 Main results and conclusions

1. The fabrication of micro cuboid and microlenses out of SZ2080™ was performed by TPL, from two different setups employing two different light sources, of same dimensions for RI measurements. A variation of the exposure dose as well as two writing methodology was analyzed: spherical spheres and concentric circles.

2. Microcuboids of 16 μm length and 8 μm height were used to retrieve the RI by IM oil method. The results showed the RI dependence on the exposure dose (from 2 mW to 4 mW) in the illumination wavelength range from 400 to 1650 nm. The results reveal that by increasing the exposure dose on the fabrication of the micro elements, a higher value of refractive index is obtained.

3. Spherical microlenses of 75 μm diameter and 5 μm thickness were fabricated with difference exposure dose (from 0.04 mW to 0.06 mW) for focal length measurements. The optical quality of the lens shows to be sufficient for optical applications by its capability of focusing and presenting high resolving power of 7 μm.

4. The presented work shows the dependence of RI (1.515 - 1.565) on exposure dose (from 0.04 mW to 0.06 mW) during fabrication of TPL in the VIS - IR wavelength range by IM method and for 632.8 nm from f measurements. The values differ from the reported $n = 1.504$ at 632.8 nm in literature for SZ2080™. The experimental values of RI concede the possibility of design and fabrication of 4D printing of free form micro elements and stacked components including GRIN element out of a single material.

References

[1] E. Skliutas, M. Lebedevaite, E. Kabouraki, T. Baldacchini, J. Ostrauskaite, M. Vamvakaki, M. Farsari, S. Juodkazis, M. Malinauskas, Polymerization mechanisms initiated by spatio-temporally confined light, Nanophotonics 10(4), 1211–1242 (2021).

[2] S. Varapnickas, M. Malinauskas, Processes of Laser Direct Writing 3D Nanolithography (Springer International Publishing, Cham, 2020), pp. 1–31.

[3] D. Wu, S.-Z. Wu, L.-G. Niu, Q.-D. Chen, R. Wang, J.-F. Song, H.-H. Fang, H.-B. Sun, High numerical aperture microlens arrays of close packing, Applied Physics Letters 97(3), 031109 (2010).

[4] C. R. Mendonca, T. Baldacchini, P. Tayalia, E. Mazur, Reversible birefringence in microstructures fabricated by two-photon absorption polymerization, J. Appl. Phys 102(1), 1–5 (2007).

[5] E. Stegenburgs, A. Bertoncini, A. Trichili, M. S. Alias, T. K. Ng, M. S. Alouini, C. Liberale, B. S. Ooi, Near-Infrared OAM Communication Using 3D-Printed Microscale Spiral Phase Plates, IEEE Commun. Mag. 57(8), 65–69 (2019).

[6] A. Žukauskas, I. Matulaitiene, D. Paipulas, G. Niaura, M. Malinauskas, R. Gadonas, Tuning the refractive index in 3D direct laser writing lithography: Towards GRIN microoptics, Laser Photonics Rev. 9(6), 706–712 (2015).

[7] A. Bertoncini, C. Liberale, 3d printed waveguides based on photonic crystal fiber designs for complex fiber-end photonic devices, Optica 7(11), 1487–1494 (2020).

[8] M. Plidschun, H. Ren, J. Kim, R. Förster, S. A. Maier, M. A. Schmidt, Ultrahigh numerical aperture meta-fibre for flexible optical trapping, Light: Science & Applications 10(1), 57 (2021).

[9] M. Schmid, F. Sterl, S. Thiele, A. Herkommer, H. Giessen, 3d printed hybrid refractive/diffractive achromat and apochromat for the visible wavelength range, Opt. Lett. 46(10), 2485–2488 (2021).

[10] Y. Li, S. Park, M. McLamb, M. Lata, S. Schöche, D. Childers, I. D. Aggarwal, M. K. Poutous, G. Boreman, T. Hofmann, UV to NIR optical properties of IP-Dip, IP-L, and IP-S after two-photon polymerization determined by spectroscopic ellipsometry, Opt. Express 9(11), 4318 (2019).

[11] S. Monneret, P. Huguet-Chantôme, F. Flory, m-Lines technique: Prism coupling measurement and discussion of accuracy for homogeneous waveguides, J. Opt. A-Pure Appl. Op. 2(3), 188–195 (2000).

[12] T. Gissibl, S. Wagner, J. Sykora, M. Schmid, H. Giessen, Refractive index measurements of photo-resists for three-dimensional direct laser writing, Opt. Express 7(7), 2293 (2017).

[13] R. J. Nussbaumer, M. Halter, T. Tervoort, W. R. Caseri, P. Smith, A simple method for the determination of refractive indices of (rough) transparent solids, J. Mater. Sci 40(3), 575–582 (2005).

[14] M. Malinauskas, G. Kiršanske, S. Rekštyte, T. Jonavičius, E. Kaziulionyte, L. Jonušauskas, A. Žukauskas, R. Gadonas, A. Piskarskas, Nanophotonic lithography: A versatile tool for manufacturing functional three-dimensional micro-/nano-objects, Lith. J. Phys 52(4), 312–326 (2012).

[15] A. Žukauskas, M. Malinauskas, G. Seniutinas, S. Juodkazis, Rapid Laser Optical Printing in 3D at a Nanoscale (John Wiley Sons, Ltd, 2016), chapter 1, 1–23.

[16] L. Jonušauskas, D. Gailevičius, S. Rekštytė, T. Baldacchini, S. Juodkazis, M. Malinauskas, Mesoscale laser 3d printing, Opt. Express 27(11), 15205–15221 (2019).

[17] A. Žukauskas, M. Malinauskas, C. Reinhardt, B. N. Chichkov, R. Gadonas, Closely packed hexagonal conical microlens array fabricated by direct laser photopolymerization, Appl. Opt. 51(21), 4995–5003 (2012).

[18] A. Ovsianikov, J. Viertl, B. Chichkov, M. Oubaha, B. MacCraith, I. Sakellari, A. Giakoumaki, D. Gray, M. Vamvakaki, M. Farsari, C. Fotakis, Ultra-low shrinkage hybrid photosensitive material for two-photon polymerization microfabrication, ACS Nano 2(11), 2257–2262 (2008).

[19] F. Flory, H. Rigneault, J. Massaneda, S. Monneret, Optical Waveguide Characterization of Thin Films., Rev. Laser. Eng 24(1), 94–102 (1996).

[20] R. Ulrich, R. Torge, Measurement of Thin Film Parameters with a Prism Coupler, Appl. Opt 12(12), 2901 (1973).

[21] S. Dottermusch, D. Busko, M. Langenhorst, U. W. Paetzold, B. S. Richards, Exposure-dependent refractive index of Nanoscribe IP-Dip photoresist layers, Opt. Lett 44(1), 29 (2019).

[22] F. Flory, G. Albrand, D. Endelema, N. Maythaveekulchai, E. P. Pelletier, H. Rigneault, Guided-wave characterization techniques for the comparison of properties of different optical coatings, Thin Films for Optical Systems 1782, 316 (1993).

[23] G. E. Saman, E. R. Hancock, Estimating complex refractive index using ellipsometry, Lecture Notes in Computer Science (including subseries Lecture Notes in Artificial Intelligence and Lecture Notes in Bioinformatics) 8156 LNCS, 201–210 (2013).

[24] H. Fujiwara, Ellipsometry, Handbook of Optical Metrology: Principles and Applications, Second Edition (1), 705–724 (2015).

[25] T. Wood, J. L. Rouzo, F. Flory, P. Coudray, V. R. Mastelaro, P. Pelissari, S. Zilio, Comparison of refractive indices measured by m-lines and ellipsometry: application to polymer blend and ceramic thin films for gas sensors, SPIE 8466, 175 – 184 (2012).

[26] M. Schmid, D. Ludescher, H. Giessen, Optical properties of photoresists for femtosecond 3D printing: refractive index, extinction, luminescence-dose dependence, aging, heat treatment and comparison between 1-photon and 2-photon exposure, Opt. Mater. Express 9(12), 4564 (2019).

[27] V. Melissinaki, M. Farsari, S. Pissadakis, A fiber optic fabry–perot cavity sensor for the probing of oily samples, Fibers 5(1), 1 (2017).

[28] A. Žukauskas, M. Malinauskas, C. Reinhardt, B. N. Chichkov, R. Gadonas, Closely packed hexagonal conical microlens array fabricated by direct laser photopolymerization, Appl. Opt. 51(21), 4995–5003 (2012).

[29] L. Jonušauskas, D. Gailevičius, L. Mikoliūnaitė, D. Sakalauskas, S. Šakirzanovas, S. Juodkazis, M. Malinauskas, Optically Clear and Resilient Free-Form μ-Optics 3D-Printed via Ultrafast Laser Lithography, Materials 10(1) (2017).

[30] R. Guo, S. Xiao, X. Zhai, J. Li, A. Xia, W. Huang, Micro lens fabrication by means of femtosecond two photon photopolymerization, Opt. Express 14(2), 810 (2006).

[31] S. H. Park, S. H. Lee, D.-Y. Yang, H. J. Kong, K.-S. Lee, Subregional slicing method to increase three-dimensional nanofabrication efficiency in two-photon polymerization, Applied Physics Letters 87(15), 154108 (2005).

[32] C. Hüttig, K. Stemmer, The spiral grid: A new approach to discretize the sphere and its application to mantle convection, Geochem. Geophys 9(2) (2008).

6 Publications and Conferences

1. Conference. Diana Gonzalez-Hernandez, Simonas Varapnickas, Mangirdas Malinauskas. Fabrication of Three-Dimensional Microelements by two-photon lithography for refractive index measurements. Open Readings, (March 19th, 2021), Vilnius, Lithuania.

2. Conference. Laser 4D printing of micro-optics by dose dependent control of refractive index. Photonics West SPIE (2022)

3. Manuscript for J. Phys. Photon. Measurements of effective optical refractive index for 3D microelements.

4. Manuscript for MDPI Photonics. Enabling laser 3D printing of micro-optics out of transparent inorganics.

Measurements of Effective Optical Refractive Index for 3D Microelements

Diana Gonzalez-Hernandez

The two-photon lithography (TPL) technique has been widely used for the fabrication of microelements for optical applications where the understanding of the refractive index (RI) of the material is fundamental. Different techniques allows the measurements of the RI of the material but they limit the dimension of the structures to 2D. Two techniques are presented for RI measurements of 3D microelements fabricated by TPL: index-matching (IM) oils and focal length measurements. The fabrication of microcuboids and spherical microlenses out of SZ2080™ by TPL. The IM oils method showed different values of RI dependent on illumination wavelength (VIS - IR range) and exposure dose during fabrication by TPL with RI in the range of 1.505 to 1.535 which differs from the RI presented in literature ($n = 1.504$) for SZ2080™ at 632.8 nm for single-photon polymerization. The microlenses present a high resolving power of 7 μm with an optical performance suitable for optical applications. The RI experimental values from focal length measurements confirm the dependency of the RI on exposure dose during TPL fabrication process. The result of this work shows the RI dependency on exposure dose and geometry and concedes the possibility of the design and fabrication of 4D printing of free form micro elements and stacked components out of a single hybrid organic-inorganic prepolymer material.

Mediciones de Indice de Refraccion Optico Efectivo de 3D Microelementos

Diana Gonzalez-Hernandez

La técnica de litografía de dos fotones (LDF) es ampliamente usada en la fabricación de micro elementos para aplicaciones ópticas donde la comprensión del índice de refracción (IR) del material es fundamental. Diferentes técnicas permiten realizar la medición del IR de materiales pero están limitadas a estructuras en 2D. Dos técnicas son presentadas en este trabajo para las mediciones de IR de micro elementos en 3D fabricados por LDP: coincidencia de indices con aceites (CI) y medición de distancia focal de micro lentes. La fabricación de micro cuboides y micro lentes esféricas del prepolímero SZ2080™ fue realizada por LDF. El método CI mostró differentes valores de IR dependiente de la longitud de onda de iluminación (rango de VIS - IR) y energía depositada durante la fabricación por LDF en un rango de 1.505 a 1.535 que difiere del presentado en literatura ($n = 1.504$) para SZ2080™ a 632.8 nm por polymerización de un solo fotón. Las micro lentes presentan un poder de resolución de 7 μm con un rendimiento óptico adecuado para aplicaciones ópticas. Los valores experimentales de IR obtenidos confirman la dependencia del IR de la energía depositada durante el proceso de fabricación por LDF. El resultado de este trabajo presenta la dependencia del IR en la energía depositada y la geometría de los micro elementos y concede la posibilidad de diseñar y fabricar micro elementos y componentes ópticos apilados de libre forma por impresión 4D usando un único pre polímero híbrido orgánico-inorgánico.